STUDY ON THE MODIFICATION OF DIFFUSER TO THE EFFECT ON AERODYNAMIC OF THE F1 IN SCHOOLS CAR

Submitted in accordance with the requirement of the Universiti Teknikal Malaysia Melaka (UTeM) for the Bachelor Degree of Manufacturing Engineering (Hons.)

by

LIM YIK SENG

FACULTY OF MANUFACTURING ENGINEERING

Year 2020/2021

DECLARATION

I hereby, declared this report entitled “Study On The Modification Of Diffuser To The Effect On Aerodynamic Of The F1 In School Car” is the results of my own research except as cited in reference

Signature : ……

Author’s Name : LIM YIK SENG

Date : 11/9/2021

APPROVAL

This report is submitted to the Faculty of Manufacturing Engineering of Universiti Teknikal Malaysia Melaka as a partial fulfillment of the requirement for the degree of Bachelor of Manufacturing Engineering (Hons.). The members of the supervisory committee are as follow:

Mohammad ridzuan Jamli

(Principle Supervisor) – Signature & Stamp

Ir. Dr. Mohamad Ridzuan Bin Jamli
Senior Lecturer
Faculty of Manufacturing Engineering
Universiti Teknikal Malaysia Melaka

ABSTRACT

F1 IN SCHOOLS is a global competition that promote exciting ways for students with the age range from 9 to 19 to study subject related with Science, Technology, Engineering and Mathematics (STEM). The goal in the competition is to finish the race on a 20 m track with the shortest time possible. There are two factors which affect the aerodynamic performance which are the drag and lift force. Drag force and extra downforce will slow down the speed of the car while extra lift force will cause imbalance of the car. Thus, study on the modification of underbody diffuser is important as it enables the control both drag and lift force of the car. Therefore, the objective of this study is to produce flow analysis on the F1 IN SCHOOLS Car. besides, this study aims to investigate the effect of diffuser angle on the drag and lift coefficient of the fast-moving car. Moreover, this study also aims to evaluate appropriate diffuser angle for maintaining suitable lift coefficient of the car. Tools that will be used in this study is by using Autodesk Fusion 360 for 3D modelling of the car and the CFD simulation will be run using Ansys Fluent. Before conducting CFD simulation for simplified 2D, 3D and complete 3D model analysis, mesh density analysis is done to obtain proper surface mesh element size that converges the result. Besides, comparison between own simulation results with previous wind tunnel test result is done to verify the fluent setting used. Ahmed body simulation result is then done to obtain the relationship between various angle of diffuser with drag and lift coefficient. The simulation results of simplified 2D, 3D and complete 3D model analysis shows different optimum diffuser angle for best aerodynamic performance. Besides, the result also shows that lift coefficient decreases as diffuser angle increases.

ABSTRAK

F1 IN SCHOOLS adalah sebuah pertandingan global yang mempromosikan pembelajaran yang menarik bagi pelajar yang berumur antara 9 hingga 19 tahun untuk mempelajari subjek yang berkait dengan Sains, Teknologi, Kejuruteraan dan Matematik (STEM). Matlamat dalam pertandingan ini adalah untuk menamatkan perlumbaan di lintasan sepanjang 20 m dengan masa sesingkat mungkin. Terdapat dua faktor yang mempengaruhi prestasi aerodinamik iaitu daya tarikan dan daya angkat. Daya tarik dan daya turun tambahan akan melambatkan kelajuan *F1 IN SHOCCLS Car* sementara daya angkat tambahan akan menyebabkan ketidakseimbangan *F1 IN SHOCCLS Car*. Oleh itu, objektif kajian ini adalah untuk menghasilkan analisis aliran pada *F1 IN SCHOOLS Car*. Selain itu, kajian ini bertujuan untuk mengkaji pengaruh sudut diffuser pada pekali tarik dan angkat pada *F1 IN SCHOOL Car* yang bergerak pantas. Di samping itu, kajian ini juga bertujuan untuk megkaji sudut *diffuser* yang sesuai untuk mengekalkan pekali angkat yang sesuai. Alat yang akan digunakan dalam kajian ini adalah dengan menggunakan *Autodesk Fusion 360* untuk pemodelan *3D F1 IN SHOCCLS Car* dan simulasi *CFD* akan dijalankan menggunakan *Ansys Fluent.* Sebelum melulakan simulasi CFD untuk analisis model 2D, 3D, dan 3D lengkap analisis, analisis kepadatan jala dilakukan untuk mendapatkan ukuran elemen permukaan permukaan yang tepat. Selain itu, perbandingan antara hasil simulasi dengan hasil ujian *wind tunnel test* dilakukan untuk mengesahkan *fluent setting* yang digunakan. Hasil simulasi *Ahmed body* kemudian dilakukan untuk mendapatkan hubungan antara pelbagai sudut *diffuser* dengan pekali seret dan angkat. Hasil simulasi analisis model 2D, 3D dan 3D lengkap menunjukkan sudut *diffuser* optimum yang berbeza untuk prestasi aerodinamik terbaik. Selain itu, hasilnya juga menunjukkan bahawa pekali angkat menurun ketika sudut *diffuser* meningkat.

DEDICATION

Only

my beloved father, Lim Boon Beng

my beloved mother, Lo Chin Liang

for giving me support mentally

my respected supervisor, Dr. Mohamad Ridzuan Bin Jamli

for giving me suggestion and informative ideas

Thank you so much

ACKNOWLEDGEMENT

I would like to thank all the person involved in assisting me to complete my final year project.

I would like the express my gratitude to my supervisor, Dr. Ridzuan Bin Jamli, who never hesitates to offer suggestion and ideas on improvement in helping me to complete the study.

Besides, I would like to appreciate my family for giving me support, money and encouragement in completing the study.

Lastly, special thanks to my friend Muhammad Nadzirul Mubin bin Abdul hamid who always share and discuss ideas regarding the content of the study.

TABLE OF CONTENT

LIST OF TABLES

LIST OF FIGURES

LIST OF ABBREVIATIONS

STEM	-	Science, Technology, Engineering and Maths
CAD	-	Computational-Aided Design
CAE	-	Computational-Aided Engineering
F1	-	Formula One
CO2	-	Carbon Dioxide
CFD	-	Computational Fluid Dymamics
RANS	-	Reynolds-averaged Navier–Stokes
SIMPLE	-	Semi-Implicit Method for Pressure Linked Equations
FVM	-	Finite Volume Method
COP	-	Coefficient of Pressure
RMS	-	Root Mean Square

LIST OF SYMBOLS

F_D	-	Drag Force
F_L	-	Lift Force
F_S	-	Side Force
T_{RM}	-	Rolling Moment
T_{PM}	-	Pitching Moment
T_{YM}	-	Yawing Moment
L	-	Length
W	-	Width
H	-	Height
α, α_d, β	-	Diffuser Angle
G_c	-	Ground Clearance
C_D	-	Draw Coefficient
C_L	-	Lift Coefficient
C_P	-	Pressure Coefficient
l_d	-	Diffuser Length
N	-	Newton

CHAPTER 1
INRODUCTION

1.1 Background of Study

F1 IN SCHOOLS is a global competition held once a year, and participants' ages range from 9 to 19. This competition offers exciting ways to learn subjects related to Science, Technology, Engineering and Maths (STEM). F1 IN SCHOOLS competition's main concern is to achieve the highest speed possible for the car to complete a race on a 20-meter track in the shortest time. To accomplish that, knowledge of fluid dynamics, aerodynamics and physic is indispensable (Mansor, 2017). There are a few parameters affect the speed of the car, which are drag force and downforce.

Drag force is resistance or forces that act on a fast-moving object with the direction opposite to the direction of motion. In FI IN SCHOOLS car, drag force that occurs can be sub-divided into two categories, which are skin friction drag and pressure drag. Skin friction drag occurs between the moving car surface and the fluid (Paturrahman et al., 2018). In other words, the surface of the F1 IN SCHOOLS Car needs to be polished to reduce the skin friction drag with the air to achieve its optimum moving speed. Pressure drag happens to be always in the opposite direction with a moving object. This happens where the pressure accumulated at the front part of the F1 IN SCHOOLS car is too much compared to the car's rear part when at high speed (Mosiężny et al., 2020). This is because air molecules collide with the front of the car and create stagnation pressure, which creates pressure that pushes the car from moving forward, resulting in slowing down the car. On top of that, there is also

a pulling force generated at the rear of the car. This situation happens due to flow separation. Flow separation plays a major role in racing cars in real life and in F1 IN SCHOOLS car. It is responsible for the major portion of the aerodynamic drag of racing cars (Hassan et al., 2014). When fluid flows through a change in geometry at high speed which the fluid inertial forces higher than the viscous forces trying to keep the fluid flow attached to the surface, flow separation occurs (Ryan T. Kell). The flow separation zone generated on the rear of the moving car creates a low-pressure zone which causes pressure drag. The rear part's pressure is much lower than the front part of the car because the air molecules cannot fill in the zone. This creates a pulling force behind the car which decreases the moving speed.

Downforce is also an essential factor that affects the speed of a car and its stability in real life. Stability is an important issue because a fast-paced car would lose its balance and the tyre would lose contact with the ground. This situation applies to F1 IN SCHOOLS car because the car is accelerated using a CO2 canister which generates high thrust force at the rear part of the car. The lift force and downforce must be balanced because the guiding thread which redirects the car direction applies pulling force at the front of the car. Imbalanced lift force of the car with the guiding thread's pulling force may create a resultant force that interrupts the acceleration. Ground effect is also another method of controlling the lift force of the car. It was discovered that large amounts of downforce could be generated from the airflow between the underbody of the car and the ground plane (SEAS, 2020). In real life, F1 car uses ground plane almost like the floor of venturi duct to generate low pressure underneath the car. The shape of the venturi duct is inverted wing profile and the airflow tunnel underneath the car is narrowing down able to accelerate the airflow under the car. This creates low pressure underneath the car in accordance with Bernoulli's principle (Gordon McCabe, 2008). In F1 IN SCHOOLS car, the ground effect needs to be examined to control the lift force on the car so that the car is always in a balanced position while moving at high speed and to minimize the friction in between the wheels and track.

1.2 Problem Statement

The main factors that affect the aerodynamic performance of F1 in SCHOOLS car are drag force and lift force.

Drag force happens when the car moving at high speed which always has the opposite direction to the motion of a car. The difference between the front part and the rear part of the car causes pressure drag while skin drag happens between the car's surface with the fluid. Flow separated zone on the rear part of the car also creates drag force to the fast-moving car. To obtain better aerodynamic performance on the car, the drag coefficient must be as small as possible while the lift coefficient must be just right. The main factors that affect the aerodynamic performance of F1 IN SCHOOLS car are drag force and lift force.

Other than that, the velocity of the car only depends on the CO2 canister that generates high thrust force at the beginning of the race and the wheels of the car are not motorised. Thus, the downforce generated on the car body must be just right. This is because excessive downforce generated will increase the friction between the car's wheels and the racing track. The imbalanced force generated on the body due to the pulling force of guiding thread and extra lift force will also interrupt the car acceleration.

To obtain better aerodynamic performance on the car, the drag force must be as small as possible while the lift force and downforce must be balanced.

1.3 Objectives

There are three objectives in this study:

- To produce airflow analysis on the F1 IN SCHOOLS Car.
- To investigate the effect of different diffuser designs on the drag and lift coefficient of fast-moving F1 IN SCHOOLS Car.
- To evaluate appropriate diffuser design for maintaining suitable lift coefficient of F1 IN SCHOOLS Car.

1.4 Scope

The main focus of this study is to improve the aerodynamic performances which is the drag and lift of the F1 IN SCHOOL Car. The software used to complete this study is 3D Computer-Aided Design (CAD) modelling software and Computer-Aided Engineering (CAE) software. The CAD software used is Autodesk Fusion 360 (educational licensed) while the CAE software used is Ansys Fluent. The solver of Ansys Fluent is based on laminar flow due to the Reynold Number of model smaller than 500 for the open channel flow. The model used for simulation is k-epsilon model.

The study is also focused on examining the effects of the ground effect produced under the fast-moving F1 IN SCHOOLS Car body. Effects on the lift and drag coefficient of the fast-moving car are also focused by using various diffuser angle. Besides that, minor study on sidepot also conducted to evaluate the effect of removing sidepot on the aerodynamic performance of car body.

1.5 Significant/Important of Study

This study provides an understanding of the behaviour of airflow on the car body. As the behaviour of airflow is different when it passes through different geometry such as an edge, plane surface, or curved surface. Besides, visualization of turbulent form at which geometry can also be done easily by examining the airflow behaviour. Turbulent will form when the air flow through a change of geometry on the body usually an edge as air particles try to stick with the surface due to its viscosity characteristics. The required part for modification to smoothen the airflow can also be determined easily by examining the airflow behaviour. After that, airflow simulation can be rerun to check the airflow behaviour after modification.

The study is also important for participants in the competition to understand and visualise the airflow on the body. After the simulation is done, they can determine the drag and lift force experienced on the fast-moving car body. Visualization pressure changes and velocity of airflow under the car body also helps them to examine the ground effect experienced under the car body. With this, adjustment can be made on the height of ground clearance for a more balanced lift force on the car body.

1.6 Organization of The Report/Thesis

The organization of the report is started by introduction, followed by literature review and lastly methodology. In chapter 1 introduction, the topic discussed are the background of the research, problem statement, objectives, scope of the research, importance of the study, and the topics' summary. Chapter 2 literature review discussed the reviews of previous research related to the importance of aerodynamic in automotive, the background of Computational Fluid Dynamics (CFD), studies related to drag and downforce on fast-moving body and studies of various modification on diffuser to the aerodynamic performance. The research objective, strategies, and findings were emphasized in the review of the diffuser related research. Chapter 3 methodology describes the planning and method

used to complete this research. The modelling of the 3D model, steps done on simplification of model, analysis, mesh refinement, and results validation is discussed in the topic.

1.7 Summary

In the chapter introduction, the background of F1 IN SCHOOLS competition is stated while the two factors that affect the aerodynamic performance of the F1 IN SCHOOLS Car were discussed. The first factor is drag force which can be categorized into skin friction drag and pressure drag. The mechanism on how skin friction drags and pressure drag affect the aerodynamic performance is discussed. The second factor is the lift force its effect on the car while at high speed. Then, problems that interrupt aerodynamic performance are further discussed regarding the car's drag and lift force during a race. The objectives and scopes of this study are also stated in detail after the problem statement. Next, the importance of this study is discussed by explaining where the outcome will be benefited. Lastly, the organization of the report is discussed.

CHAPTER 2
LITERATURE REVIEW

2.1 Importance of Aerodynamics in Automotive

The employment of concepts of automotive aerodynamics has been emphasized in early 1920. Engineers at that time have begun to examine and study the automobile shape to reduce aerodynamic drag experienced on the vehicle body at higher speed. The effect of aerodynamics on vehicle is consist of forces and moments composed by three forces and torques on the x, y and z, axis. The forces and moments are also known as six aerodynamic component forces which consist of drag F_D, lift F_L, side force F_S and rolling T_{RM}, pitching T_{PM}, yawing T_{YM} moment shown in *Figure 2.1*.

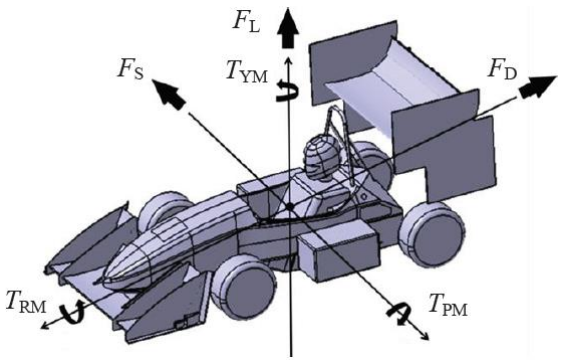

Figure 2.1: Diagram of six aerodynamic component forces (Wang et al., 2018)

2.2 Computational Fluid Dynamics (CFD)

2.2.1 Background

Computational Fluid Dynamics (CFD) has been started in the early of 1960 and it has been recognized as the combination of physic, computer science and also numerical mathematics to simulate behaviour of fluid flow on a body. In other words, CFD is an aerodynamic analysis in the form of digital. It provides a detailed understanding of fluid flow around or through a vehicle, as well as a wide range of other analyses.

The emergence of CFD in the 1965–2005 period depended on a combination of advances in computer power and algorithms. At the early development of CFD from 1960-1970, equations used in CFD are Godunov's theorem in numerical analysis and computational fluid dynamics suggested by S. K. Godunov (Jameson, 2012). From 1970 to 1980, non-linear potential flow equations were involved. The equations are type-dependent differencing by Murman-Cole, complete airplane solution by Glowinsky, multigrid technique by Brandt, complex characteristics method by Garabedian and rotated difference by Jameson. From 1980 to 1990, Euler and Reynolds-averaged Navier-Stokes (RANS) Equations were involved (Jameson, 2012). Euler equations by Leonhard Euler are sets of equations used in fluid dynamics in governing adiabatic and zero viscosity fluid (inviscid flow) (*Euler Equations (Fluid Dynamics), n.d.*). For RANS equations, the equation describes the flow of incompressible fluids with partial differential equation in fluid mechanics (William L.Hosch, 2020). Khalil (2012) states that there are a few problems faced by the CFD in early 1986. The main problems facing the CFD at that time were mainframe computational restriction; the control of irregular boundary and wall conditions with a simple orthogonal grid is difficult; the convergence and numerical diffusion is slow; the three-dimensional complex geometries are difficult to carry out; time-related calculations are still in the cradle. The development of governing equations used in CFD is shown in *Figure 2.2*.

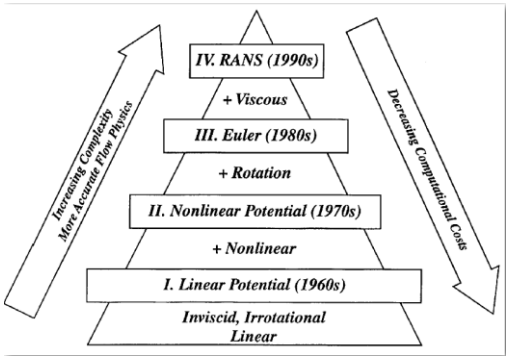

Figure 2.2: Hierarchy of Governing Equations (Jameson, 2012)

In 1990-2000, studies of CFD focused on aerodynamic shape optimization by referring to the theory of adjoint-based control. In 2000-2010, the implementation of the Discontinuous Galerkin Finite Element Method further improves the result of CFD. This method merges the benefits of utilizing hexahedral mesh, where the complexity of the generated pipeline is much lesser than the tetrahedral case (Plis et al., 2018). Nowadays, applications of aerodynamics include most body that experiences aerodynamic forces in fluid flow. For example, general applications such as fixed-wing or rotary-wing aircraft, wind turbines and propellers, ground and marine vehicles, internal flows, avian and insect flight, and atmospheric flows (ILLINOIS, 2020).

2.3 Drag

Drag force experienced on a fast-moving body is a force that has the opposite direction of the body's motion thus creating a pulling force to slow down the moving body (S. J. Lim, 2017). Aerodynamic drag experienced on a moving body is categorized into two which are pressure drag and friction (viscous) drag (Abu Mansor & Harun, 2018; Kell, 2009a; Mierzejewska et al., 2018). Pressure drag occurs depending on the geometrical structure of the moving body through the fluid, while skin friction drag depends on the friction between the moving surface and a viscous fluid (Abu Mansor & Harun, 2018).

2.3.1 Skin friction drag

Zhang et al. (2020) reported that when an object moves in fluids, for example, air or water, skin frictional drag is primarily produced in the place where turbulence usually happens in the thin layer of fluid closed to the object surface. This can be changed by controlling the geometrical structure of the near-wall turbulent boundary layer. With the development of identification technology and measuring investigation technology in fluid mechanics, the structure of the fluid layer is continuously analysed as shown in *Figure 2.3*.

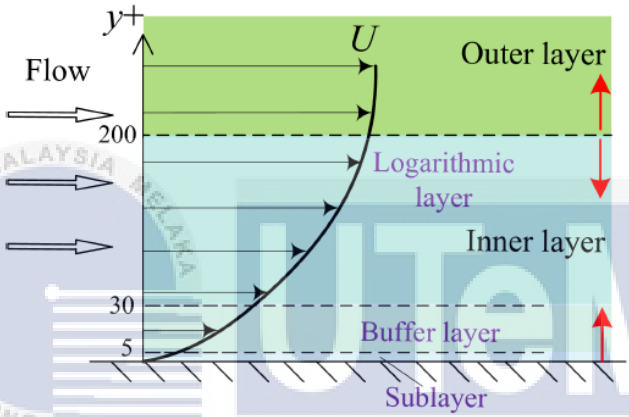

Figure 2.3:The structure of turbulent boundary layer (Zhang et al., 2020)

The turbulent boundary layer experienced on a moving body consists of the inner layer and outer layer. There are three layers in the inner layer named sublayer, buffer layer and logarithmic layer. To minimize skin friction drag, numerous drag reduction methods have been carried out. The proven effective method in reducing skin friction drag is by utilizing riblet drag reduction (Corke & Thomas, 2018; G. Yunqing, L. Tao, M. Jiegang, S. Zhengzan, 2017). Takahashi et al. (2019) also reviewed that the implementation of riblet surface on moving body shows reduction on skin friction drag even though the reduction is relatively small compared to modification on body structure in reducing pressure drag. Fu et al. (2017) explained that the turbulent-flow forms vortices above riblet surface and they remain above the riblets. This causes vortices to interact with the tips of riblet only. The chances of high-velocity vortices flow in the valleys of the riblets have been reduced and leads to high-shear stresses take place mainly on the tips of riblet. In contrast, lower velocity

fluid flow inside the valley causes the builds up of low shear stress in the riblet's valley by keeping the vortices above the riblet tips. In short, lesser momentum transfer and shear stress occur on the riblet surface and leads to a reduction of skin drag. Furthermore, Huluka & Kim (2020), studied the effect of different air duct size on the same Ahmed body and found that the friction drag on the Ahmed body can be reduced with smaller surface area of air duct.

2.3.2 Pressure drag

S. J. Lim, (2017) mentioned that pressure drag is a drag force that acts in the opposite direction to a vehicle's moving direction. The happening of this situation unpreventable and it generates a pulling force that tends to pull the vehicle from moving forward hence slows down the vehicle. The main reason of generation of pressure drag on a fast-moving vehicle are the huge pressure difference between the front and rear part of the vehicle, and the flow separation zone that happens at the rear part of the vehicle (Abu Mansor & Harun, 2018; S. J. Lim, 2017). The huge pressure difference between the front and rear of the vehicle is due to the stagnation of air molecules at the front of the vehicle and causes the pressure at the front to increase. As a result, drag force is generated to slow down the moving vehicle (Abu Mansor & Harun, 2018).

Another reason explained by Kell (2009) that increases the pressure drag is the existence of flow separation zone at the rear part of moving vehicle. This is due to the air molecules not able to stay with the car surface, creating a low-pressure zone and pulling force is generated at the rear part of the vehicle (Abu Mansor & Harun, 2018). The phenomenon can be explained by the fluid flows over a change in geometry (such as edges or corners) at high speed, inertial forces experienced by the fluid at such speed are much greater than the viscous forces of fluid. The fluid unable to attach to the surface with geometrical changes hence low-pressure zone is generated.

Various research has been done to reduce pressure drag on a fast-moving vehicle. Huluka & Kim (2020) study shows that vehicle model with installed air duct redirects

airflow to the rear part of the model. This decreases the momentum loss of rear flow and causes reduction of pressure drag due to recirculation of pressure at the lower part of rear base. Besides, pressure intensity at the front part of model vehicle decreases. This is because stagnation of air molecules at the front flows into the air duct, pressure difference between the front and rear decreases, hence pressure drag decreases. Besides, Mosiężny et al. (2020) stated that the installation of cab-roof fairing on truck provides better streamline profile to the head of truck. With the installed cab-roof fairing, airflow is redirected to the top and eliminated the flow separation zone above the truck cabin. While Kim et al. (2017) done modifications on cab-roof fairing and shows reduction of drag close to 18 % compared with the original. Hwang et al. (2016) also reported that installation of side skirt on a 15-ton truck and 40-foot trailer heavy vehicle shows a drag reduction close to 5 % compared with the same model without side skirt. However, excessive drag reduction on vehicles may increase the aerodynamic lift and the generated upward force will cause the wheels to lose contact with the ground.

2.4 Downforce

The application of aerodynamic lift is widely applied in the aerospace industry to generate lift force on the wings to lift the plane when it reaches a certain speed. In contrast, the concept of negative lift (downforce) is applied to race cars, especially in F1 industry to generate downforce on the vehicle. In general, downforce is a reaction force acts on the vehicle body and to ensure the wheels always in-contact with the track to prevent the vehicle body from losing balance at high speed (Abu Mansor & Harun, 2018). According to Feng et al. (2020), the aerodynamic package for increasing the downforce coefficient on a race car are front-wheel deflectors, front lip, side skirts, rear spoiler, and rear diffuser.

Eftekhari et al. (2020) study showed the effect of modifying the shape and setting the angle of spoiler in improving the negative aerodynamic lift while (Lee & Kim, 2019) compared the difference between flow discharged and undischarged spoiler and showed that undischarged spoiler has higher downforce compared to the discharged spoiler. (Huminic &

Huminic, 2020) reported that the downforce of a vehicle with a curved diffuser has outstanding downforce compared to a vehicle with a plane diffuser. The downforce increases as the diffuser angle and length increase. The increase of average downforce studied is 22 %.

Furthermore, theoretical approach was also applied to the vehicle to increase the downforce. Kell (2009) stated that venturi tunnel build under vehicle body produces a venturi effect that speeds up the fluid flow under the body. This reduces pressure underneath the vehicle body which can be explained by Bernoulli's principle and generates downforce on the body. Singh et al. (2020) research showed that the Bernoulli's effect underneath of a vehicle is enhanced due to the ground movement moving opposite to the vehicle hence generating pull on the air underneath the vehicle and cause the velocity of air to be faster. According to Bernoulli's principle, fluid move with higher speed has lower pressure than lower speed fluid. This enhanced the downforce on the vehicle. Dong et al. (2020) showed that the ground effect applied on high-speed trains has a critical effect on downforce generation. The decrease of ground clearance of the train body showed an increasing trend on the downforce (Takahashi et al., 2019). Džijan et al. (2019) researched the effect of rake angle on the generation of downforce by modifying the front ground clearance and the rear ground clearance on a vehicle body. The modification of ground clearance is in the range of 60 mm - 140 mm. Results showed squatting car (front ground clearance > rear ground clearance) generates largest positive lift force coefficient of 0.37. In contrast, nose-diving car (rear ground clearance > front ground clearance) generates lowest lift force coefficient of -0.21.

2.5 Diffuser

Underbody diffuser is an add-on aerodynamic device installed on rear part of vehicle (Hu et al., 2011). The purpose of diffuser is to redirect fluid flow under vehicle body into low pressure zone which generates pull on the rear part of fast-moving vehicle. It creates a pressure recovery at the rear part of vehicle body, back to the free stream pressure (Huminic & Huminic, 2020). Besides that, the influence of diffuser to the overall downforce generation

also has significant effect on a fast-moving vehicle. The list of parameters that would affect the performance of underbody diffuser includes the diffuser angle, shape, number of separators, etc (Hu et al., 2011).

Abid et al. (2017) analysed the effect of an aerodynamic downforce package for formula student race car and showed that underbody diffuser able to generate downforce on moving vehicle. The CFD analysis is carried out using ANSYS CFX software. Underbody diffuser used in the study is modified into three different diffuser angles: 12 °, 14 ° and 16 °. The distance between ground and underbody is kept constant at 38 mm throughout the analysis. The simulation is carried out using following boundary conditions as shown in Table 2.1: Boundary conditions for diffuser analysis (Abid et al., 2017)Table 2.1. Streamline and pressure contours across the diffuser is shown in Figure 2.4. From the analysis, diffuser with angle of 14 ° generates the highest downforce and drag force which are 84.8 N and 115.6 N respectively. Besides, simulation of vehicle alone is done to compared with different aerodynamic downforce package and the result is shown in Table 2.1.

Table 2.1: Boundary conditions for diffuser analysis (Abid et al., 2017)

Inlet velocity	20 m/s
Outlet average relative pressure	0 Pa
Rotating wall (tires)	82.88 rad/s
Moving wall velocity (ground)	20 m/s

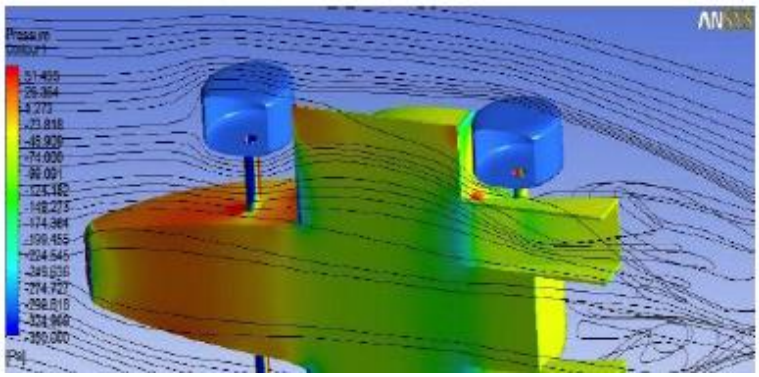

Figure 2.4: Streamlines and pressure contours across the diffuser (Abid et al., 2017)

Table 2.2: Comparison of various vehicle set up (Abid et al., 2017)

Setup	Downforce (N)	Drag (N)
Vehicle alone	11.2	109.0
Vehicle with diffuser	84.8	115.6
Vehicle with wings	580.1	305.7
Full downforce package	634.9	314.1

From the results shown in Table 2.2, we can see that vehicle with diffuser showed increment of downforce from 11.2 N to 84.8 N which is an increment of 73.6 N. Besides, it is shown that wings increase the drag force drastically to 580.1 N. However, drag force has the same trend with downforce where the increases of downforce will also increase the drag force on the vehicle.

Furthermore, Sucipto & Widodo (2018) researched on the multiple-channel under body diffuser on a rear bus body by comparing four different channel which are plane, two channel, three channel and four channel diffuser. The study used commercial CFD for numerical analysis of incompressible turbulent flow. RANS equations were used to solve the k-epsilon turbulent model and Semi-Implicit Method for Pressure Linked Equations

(SIMPLE) algorithm is used to work on pressure and velocity coupling in the simulation. The bus model and its dimension is shown in Figure 2.5 and Table 2.3 respectively, while domain of the simulation is shown in Figure 2.6. Reynolds number applied in the simulation is 2.19×10^6 which acquired from the bus length and inlet velocity. Results obtained from the simulation is shown in Figure 2.7.

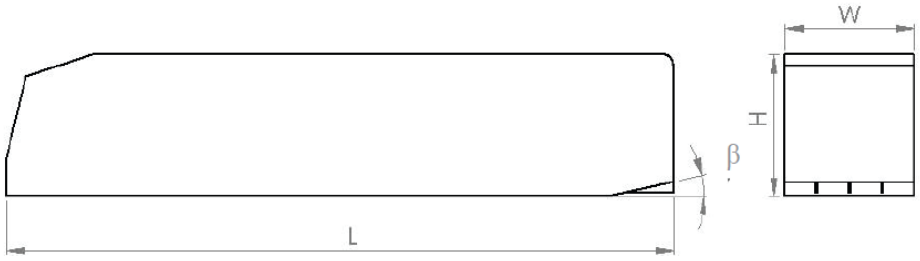

Figure 2.5: Schematic of the bus model (Sucipto & Widodo, 2018)

Table 2.3: Bus model dimension (Sucipto & Widodo, 2018)

Length (L)	11820 mm
Width (W)	2550 mm
Height (H)	3255 mm
Diffuser Angle (β)	12 °
Ground Clearance (Gc)	330 mm
Number of Channel	2, 3 and 4

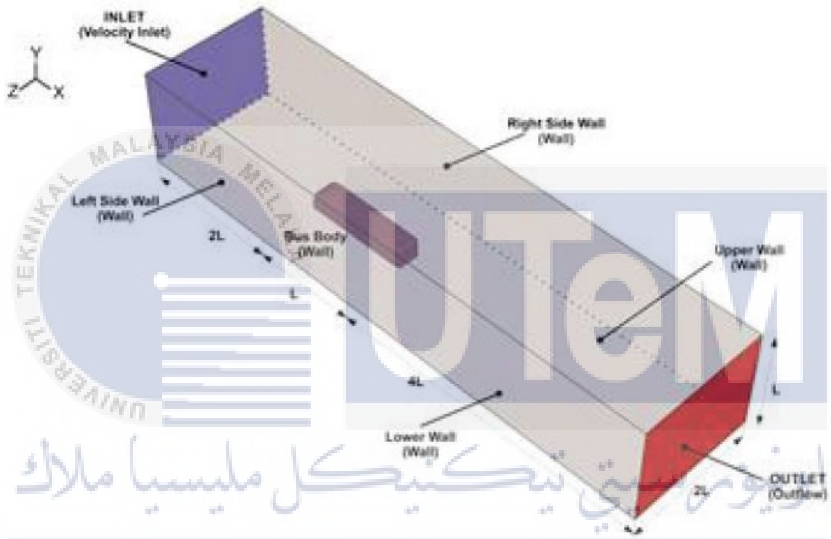

Figure 2.6: Domain and boundary condition of simulation (Sucipto & Widodo, 2018)

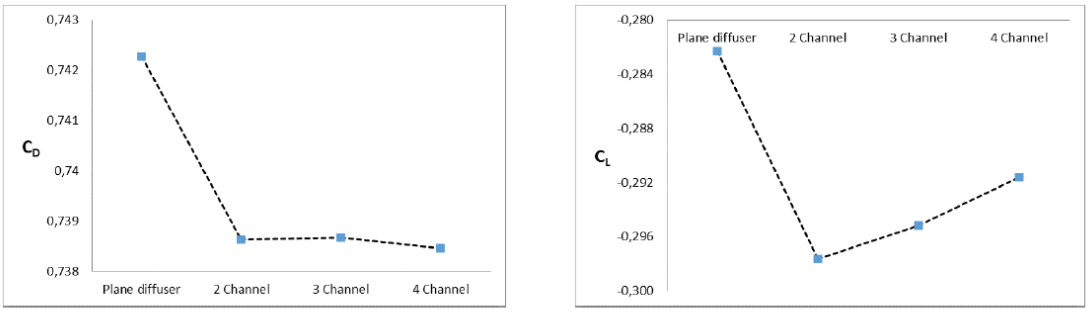

(a) (b)

Figure 2.7: Aerodynamic performance. (a) Drag coefficient, (b) Lift coefficient (Sucipto & Widodo, 2018)

Based on Figure 2.7, multiple channel diffuser shows better performance in decreasing the drag compared to plane diffuser ($C_D = 0.7422$) where the drag coefficient has reduced nearly 0.51 % on the four-channel diffuser ($C_D = 0.7384$) by producing better pressure recovery at the rear part of bus model. Besides, two-channel diffuser (C_L = -0.298) produce the lowest lift coefficient about 5.44 % compared to plane diffuser (C_L = -0.282) while increment of lift is shown on the three and four-channel diffuser.

Research regarding curved underbody diffuser was done by Huminic & Huminic (2020) to evaluate results of aerodynamic of the Ahmed body with curved underbody diffuser in terms of lift coefficient and drag coefficient. The CFD simulation is performed by ANSYS CFX using bluff body of Ahmed which has dimensions shown in Figure 2.8.

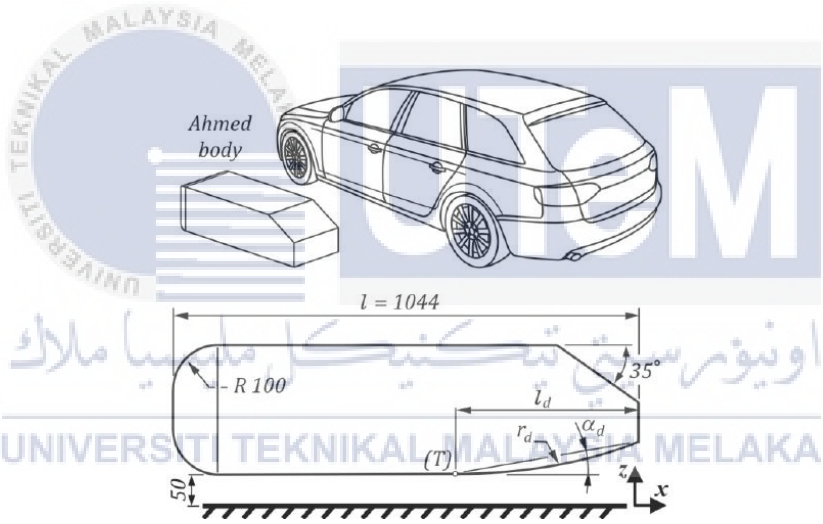

Figure 2.8: Ahmed body. 3D view and lateral view (dimensions in mm) (Huminic & Huminic, 2020)

The velocity of air was set to 40 m/s and Reynold's number is set to 2.36×10^6 based on the dimension of the Ahmed body. Ground clearance is set to 50 mm in the simulation.

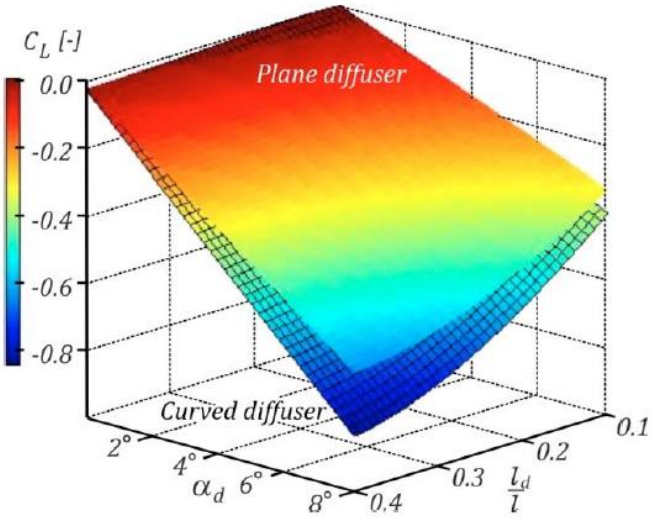

Figure 2.9: 3D maps of C_L for plane diffuser (surface without grid) and curved diffuser (surface with grid) (Huminic & Huminic, 2020)

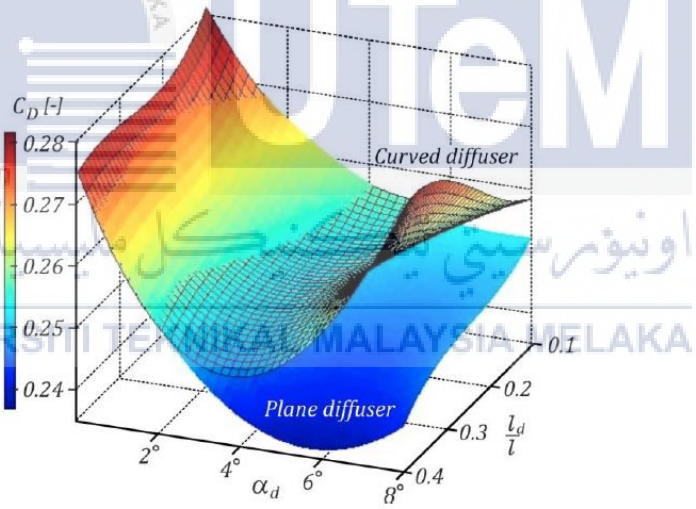

Figure 2.10: 3D maps of C_D for plane diffuser (surface without grid) and curved diffuser (surface with grid) (Huminic & Huminic, 2020)

As shown in Figure 2.9, the overall lift coefficient generated by curved diffuser is lower than plane diffuser. The lift coefficient of the body decreases as the diffuser angle and its length decrease. The minimum value of C_L for plane diffuser and curved diffuser are -0.645 and -0.814 respectively (change of C_L = 26.2 %). For the drag coefficient as shown in Figure 2.10, plane diffuser provides overall lower drag compared to curved diffuser. For

smaller angles ($a_d = 2\,°, 4\,°$), the curved diffuser has smaller drag generated compared to plane diffuser. In Figure 2.11, the result showed pressure recovery under the Ahmed body for $a_d = 4\,°$ and $l_d = 0.21$. It is shown that pressure recovery for the curved diffuser showed inflexion point of cp due to the "no edge" profile which leads to larger downforce generation compared to plane diffuser.

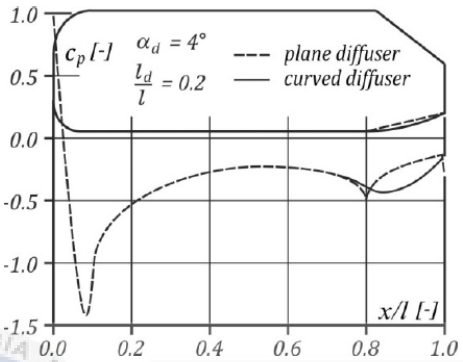

Figure 2.11: Variation of C_P in the symmetry plane for a_d = 4 ° and $l_d = 0.21$ (Huminic & Huminic, 2020)

Besides, modification of diffuser angle is done by a few researchers and the finding is reviewed. Rakibul Hassan et al. (2014) performed analysis to examine the drag of a car and modifications done to reduce drag by reducing the separation zone formed on rear part of the car. Finite Volume Method (FVM) is used to solve the Favre-average Navier-Stokes equations supported by k-epsilon turbulence model. The research is carried out at different angles of diffuser at 2.5 °, 5.0 °, 10.0 °, 12.5 ° and a 12.5 ° underbody diffuser as shown in Figure 2.12 (a) and Figure 2.12 (b) respectively. Figure 2.13 showed the flow separation at the rear part of car decreases as the value of β increases.

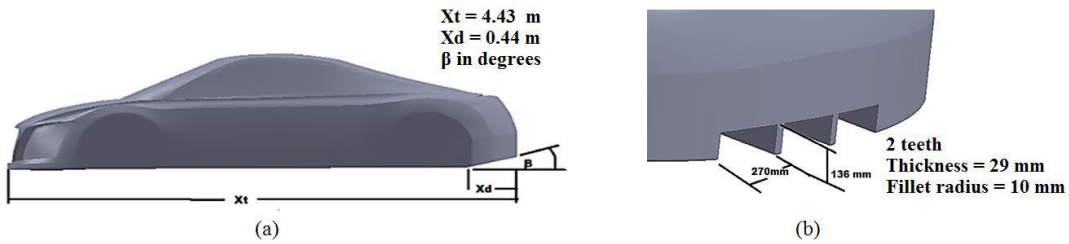

Figure 2.12: (a) Rear under-body slicing at angle B degree. (b)Rear body diffuser (Hassan et al., 2014)

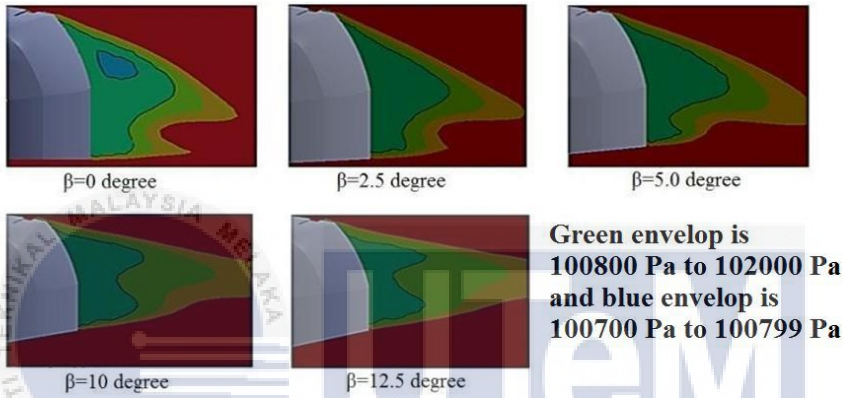

Figure 2.13: Pressure contour at the rear end (base) of car at different β, showing reduction of low-pressure zone (green) with increasing β (Hassan et al., 2014)

Table 2.4: For rear under-body modification, drag reduction at flow velocity 50 m/s (Hassan et al., 2014)

Modification	Description of modifications	C_D	ΔC_D	% of reduction of C_D
none		0.3233	-	-
Modification 1	$\beta = 2.5$ °, rear under-body sliced	0.3083	0.01500	4.639
Modification 2	$\beta = 5.0$ °, rear under-body sliced	0.2962	0.02707	8.373
Modification 3	$\beta = 10.0$ °, rear under-body sliced	0.2694	0.05386	16.58
Modification 4	$\beta = 12.5$ °, rear under-body sliced	0.2517	0.07156	22.13
Modification 5	$\beta = 12.5$ °, under-body diffuser	0.2926	0.03070	9.5

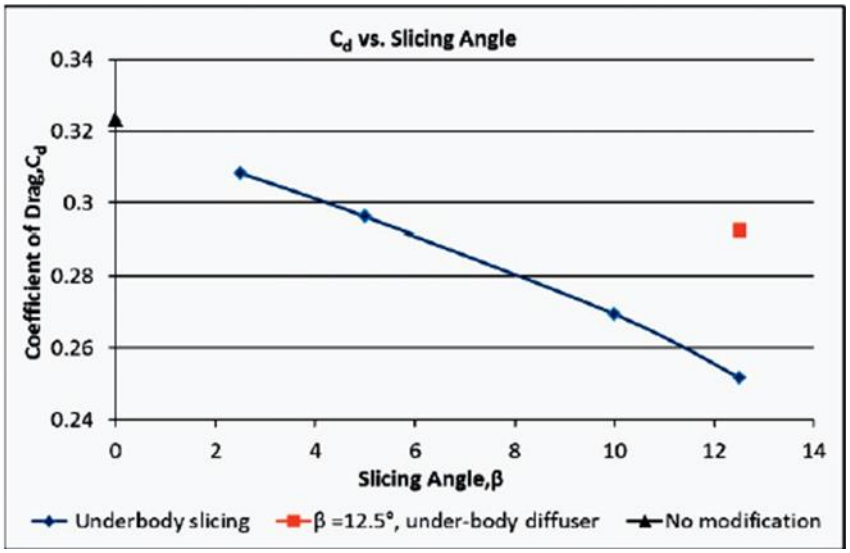

Figure 2.14: Change in C_D due to different modification (Hassan et al., 2014)

The results obtained from the simulation is shown in Table 2.4 and Figure 2.14. At $\beta = 2.5\,°$, the value of C_D is reduced by 4.639 % compared to C_D at $\beta = 0\,°$. As the value of β increases to $12.5\,°$, the percentage reduction of C_D increased to 22.13 % while modification 5 shown in Figure 2.12 (b) which has the same diffuser angle only showed percentage reduction of C_D equals to 9.5 %. Thus, the result from simulation showed that diffuser with higher angle will produce lower drag on the car.

The result of experimental investigation on different diffuser angles done by Moghimi & Rafee (2018) on aerodynamic behaviour of Ahmed body show different trend on drag coefficient. The research focused on studying how diffuser improve aerodynamics and how diffuser affect the separation flow generated behind the body. FVM is used to perform numerical simulations by solving the RANS equations in the simulation. The Reynolds number for the simulation was 9.31×10^4 based on the dimensions of model and speed flow in the wind tunnel. Original dimension of standard Ahmed body is shown in

Figure 2.15 while modification done on the body is shown in Figure 2.16 at different diffuser angles which are 0 °, 4 °, 8 °, 12 °, 16 ° and 20 °

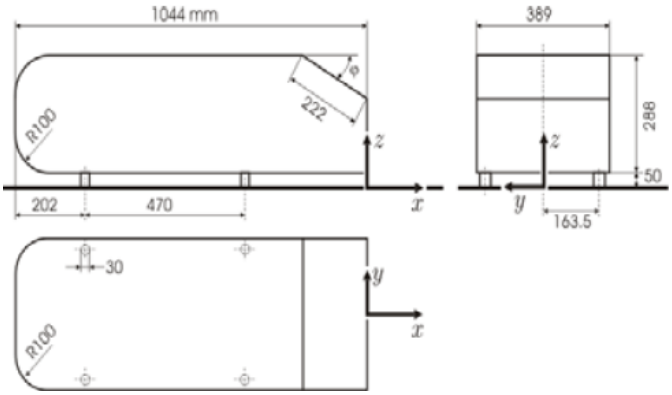

Figure 2.15: Standard Ahmed body geometry (all dimensions in mm) (Moghimi & Rafee, 2018)

Figure 2.16: Diffuser angle (α) and length (L) on the geometry, flow direction over the body shown by parallel arrows (Moghimi & Rafee, 2018)

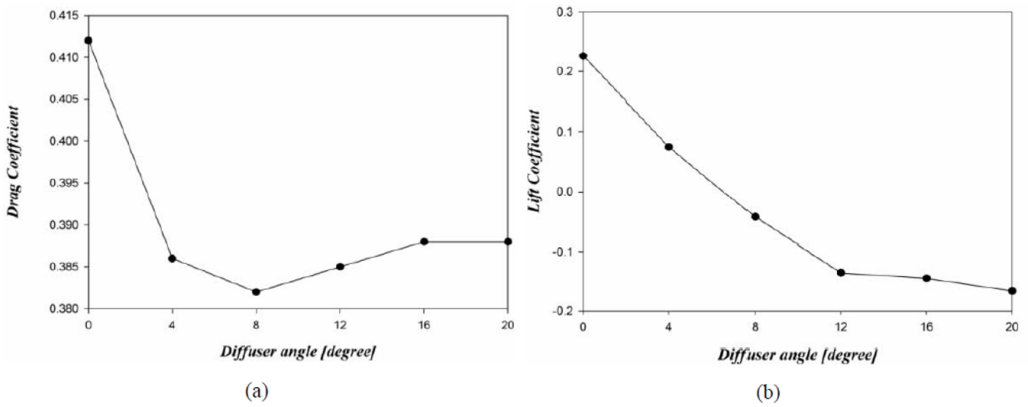

Figure 2.17: Variation of the lift and drag coefficient vs. diffuser angle, (a) Drag coefficient (C_D), (b) Lift coefficient (C_L) (Moghimi & Rafee, 2018)

From Figure 2.17 (a), it is shown that diffuser angle at 8 ° generate the lowest drag coefficient of 0.382 but increment is shown as the diffuser angle increases to 16 ° while diffuser angle of 20 ° shows similar drag coefficient with diffuser angle of 16 °. Besides, the result for lift coefficient shows decreasing trend with the increase of diffuser angle as shown in Figure 2.17 (b). The lowest lift coefficient of -0.17 is achieved on diffuser angle of 20 °.

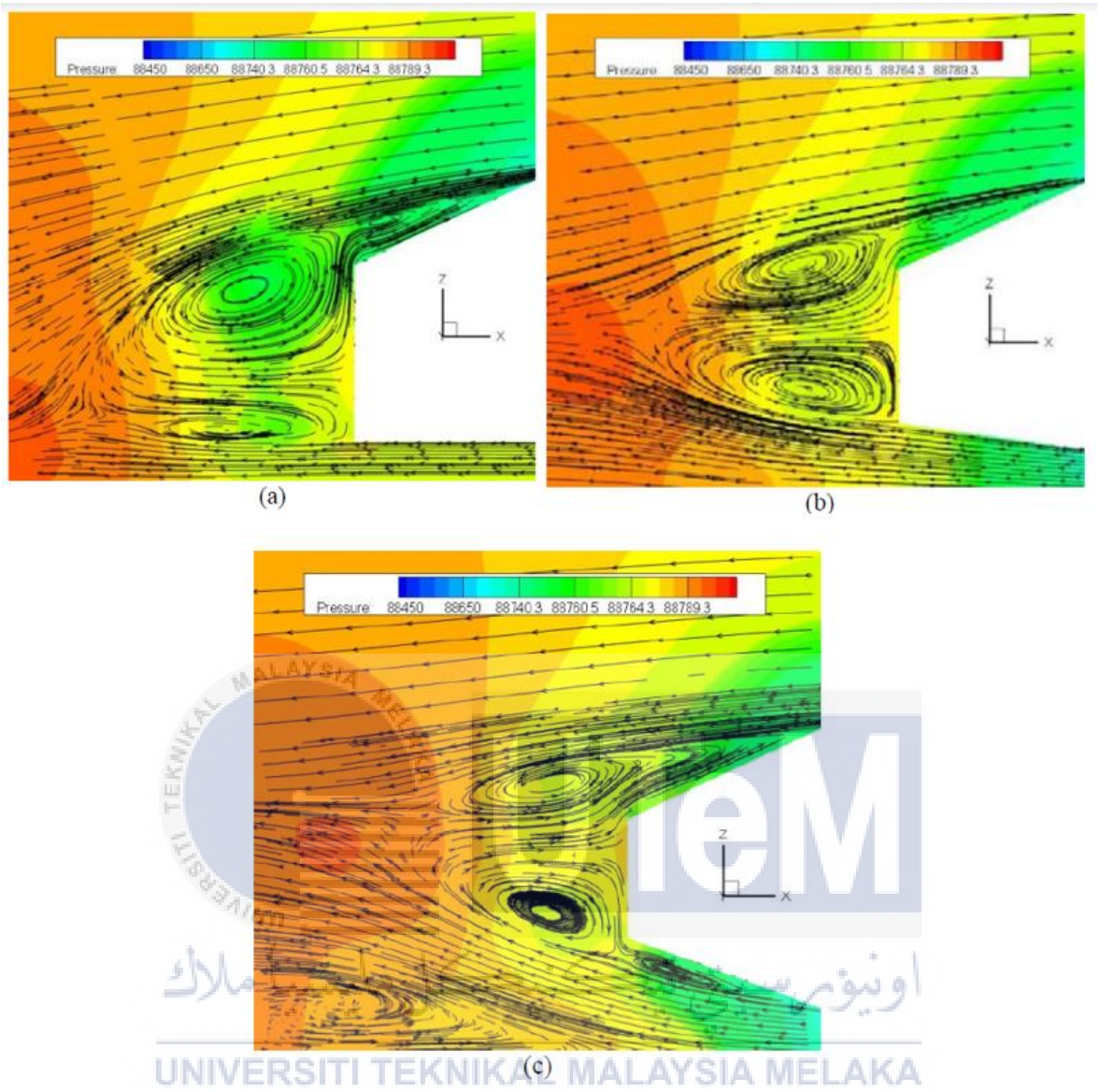

Figure 2.18: Flow pattern at the symmetry plane behind the body showing the size of low pressure (recirculating flows), (a) 0 degree, (b) 8 degrees, (c) 20 degrees -pressure contours in [Pa] (Moghimi & Rafee, 2018)

Based on Figure 2.18, it is shown that low pressure zone behind the body is recovered as the diffuser angle increases from 0 ° to 20 °. The decrease in size of low-pressure zone behind the body leads to lower drag on body and the pressure difference between the front and rear part of body is reduced. However, the increase of drag coefficient as shown in Figure 2.17 (a) is influenced by flow separation generated on the diffuser itself. Based on Figure 2.19 (a), there is no flow separation zone generated at diffuser angle of 8 °. However, at diffuser angle of 20 °, flow separation zone is generated due to the trailing edge on the

diffuser as shown in Figure 2.19 (b). This cause low-pressure generated at the rear part of body and raises the drag coefficient.

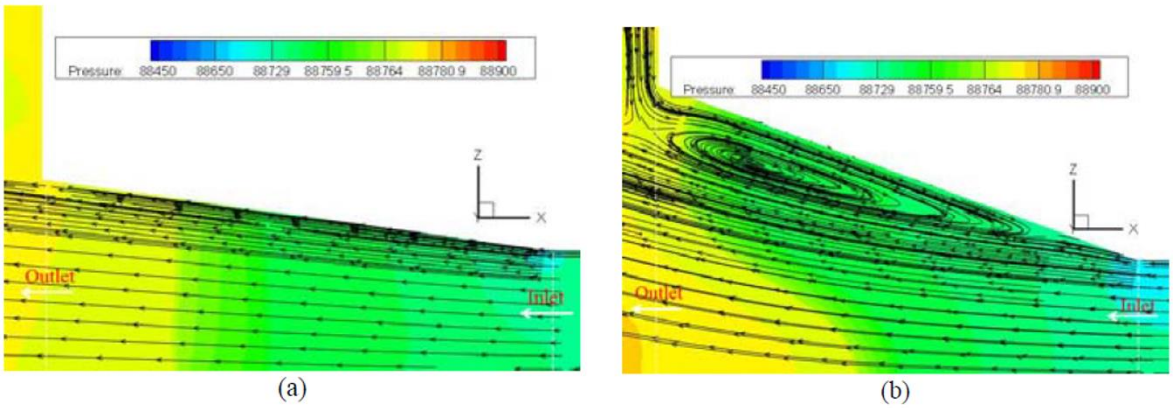

Figure 2.19: Flow separation at higher diffuser, (a) 8 degrees and (b) 20 degrees -pressure contours in [Pa] (Moghimi & Rafee, 2018)

Research done by Hu et al. (2011) showed same trend with experimental investigation done by (Moghimi & Rafee, 2018) where the drag coefficient decreases at lower diffuser angle and increases at higher diffuser angle. The research aims to study the effect of different diffuser angle on a sedan. Numerical simulation for the research is done using software FLUENT. The sedan model is simplified to reduce the simulation period as shown in Figure 2.20, side mirror, underbody transmission and front grille is eliminated from the sedan model. The dimension of sedan model is 4829 mm × 1888 mm × 1458 mm and ground clearance are kept constant on 210 mm for the simulation. In this research, five different diffuser angles were examined which are 0 °, 3 °, 6 °, 9.8 ° (original model diffuser angle) and 12 °. The configuration on sedan's diffuser angle is shown in Figure 2.21.

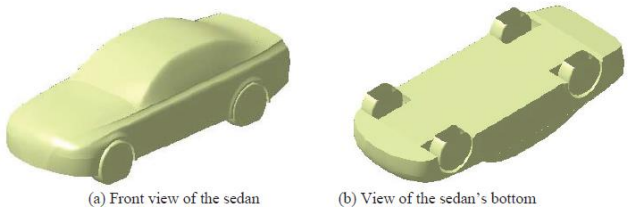

Figure 2.20: Geometric model of original model (Hu et al., 2011)

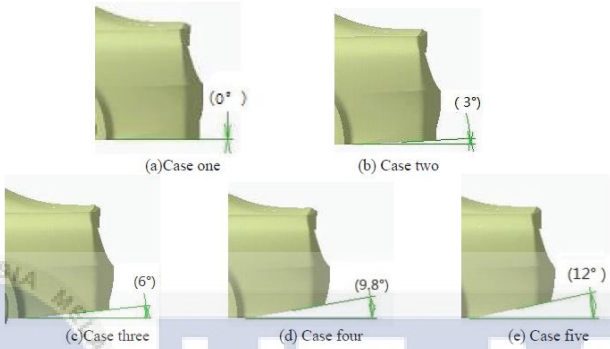

Figure 2.21: Rear part configurations of automobile for various diffuser angles (Hu et al., 2011)

Table 2.5: Total drag and lift coefficient for various diffuser angles (Hu et al., 2011)

Case name	Diffuser angle	C_D	C_L
Case one	0 °	0.2841	0.3350
Case two	3 °	0.2718	0.2791
Case three	6 °	0.2487	0.2656
Case four (original model)	9.8 °	0.2673	0.2633
Case five	12 °	0.2822	0.2586

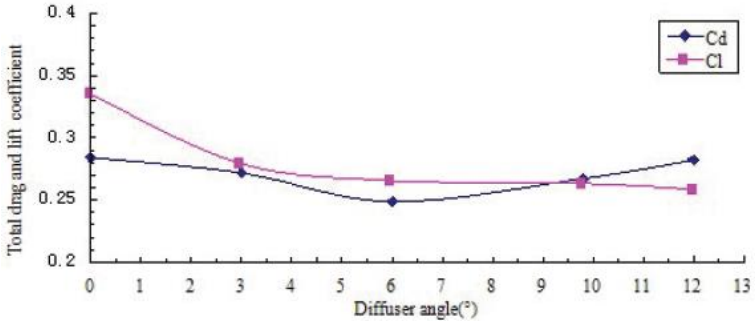

Figure 2.22: Total drag and lift coefficient versus diffuser angle (Hu et al., 2011)

Based on Table 2.5 and Figure 2.22, the drag coefficient decreases for diffuser angle of 3 ° and 6 ° but increases at diffuser angle of 9.8 ° and 12 °. Minimum drag coefficient achieved is 0.2487 at diffuser angle of 6 °. However, the lift coefficient showed decreasing trend as the diffuser angle increases similar to research done by Moghimi & Rafee (2018) and the minimum lift coefficient achieved is 0.2586 at diffuser angle of 12 °.

Sreeradh (2018) also did research on modifying the diffuser angle of sedan and the purpose of research is to examine the flow structure on the sedan with different diffuser angles. The sedan model was designed using Creo Parametric 2.0 modelling software and it is imported to ANSYS fluent for numerical simulation. The fluid density and viscosity for the simulation is set to 1.2256 kg/m^3 and 1.714X10-5 kg/ms respectively. Velocity of inlet fluid and outlet pressure were set to 100 m/s and 1 bar respectively. Top and bottom of geometries were set to wall boundaries. The diffuser angle is modified to 7 °, 8 ° and 9.8 ° for three different cases of simulation. The coefficient of pressure, COP and fluid flow velocity for three different cases is shown from Figure 2.23 to Figure 2.28

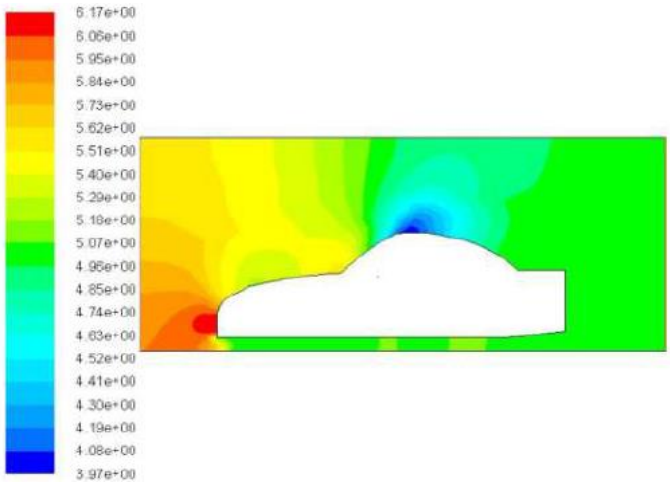

Figure 2.23: COP for 7 ° diffuser angle (Case 1) (Sreeradh, 2018)

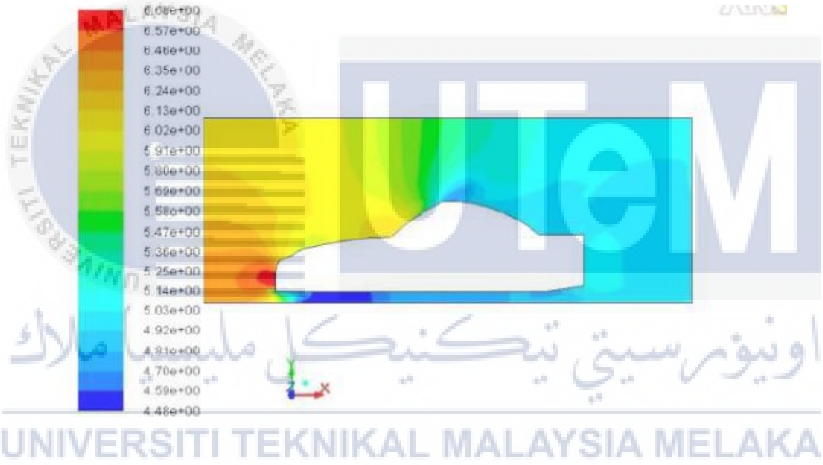

Figure 2.24: COP for 8 ° diffuser angle (Case 2) (Sreeradh, 2018)

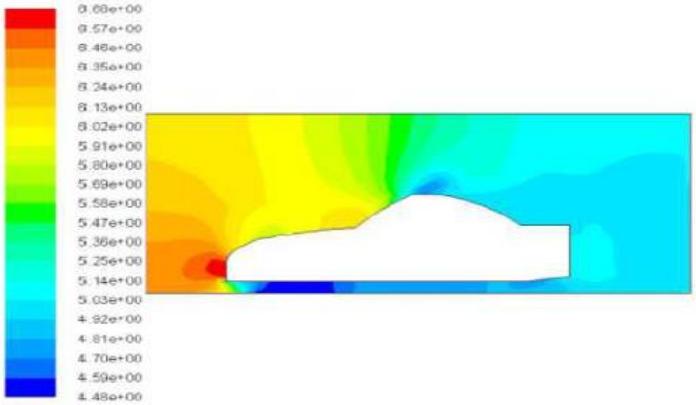

Figure 2.25: COP for 9.8 ° diffuser angle (Case 3) (Sreeradh, 2018)

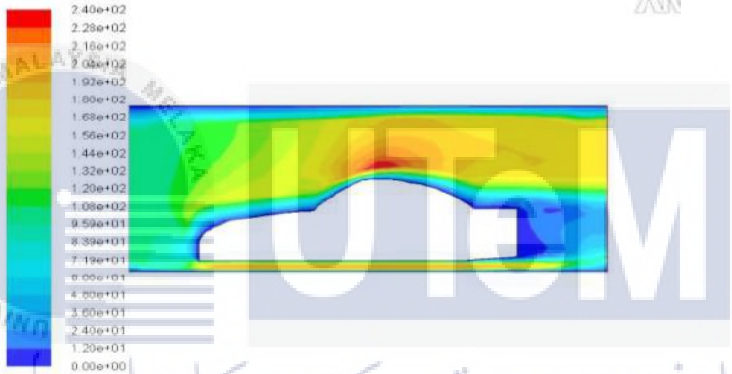

Figure 2.26: Velocities for 7 ° diffuser angle (Case 1) (Sreeradh, 2018)

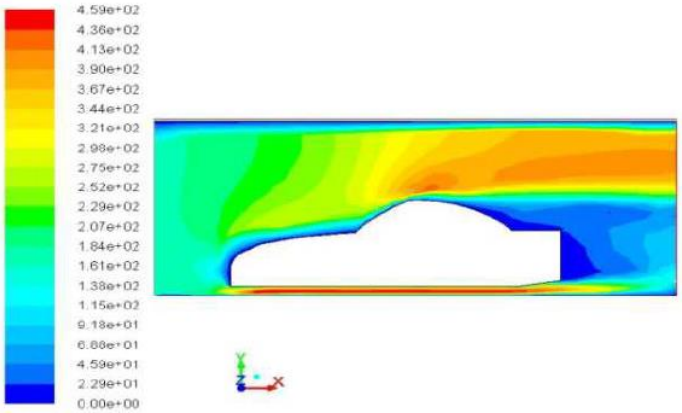

Figure 2.27: Velocities for 8 ° diffuser angle (Case 2) (Sreeradh, 2018)

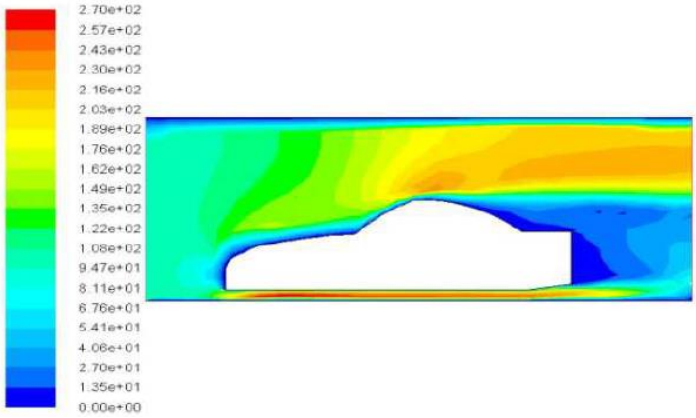

Figure 2.28: Velocities for 9.8 ° diffuser angle (Case 3) (Sreeradh, 2018)

Based on Figure 2.23 to Figure 2.25, it is shown that the velocity of airflow under sedan's body became faster as the diffuser angle increases. This generates low pressure zone under the sedan's body. The difference of pressure between the upper part of body and under the body for three different cases can be seen from Figure 2.26 to Figure 2.28. The pressure difference become greater as the diffuser angle increases. The lowest pressure occurs on under body of Case 2 and Case 3 where the value of pressure is 4.48 bar. As the pressure difference between the upper part and under body increases, larger downforce is generated in the body. In velocity case, it is shown that diffuser angle of 8 ° has higher velocity on under body compared to diffuser angle of 9.8 °. The maximum velocity for diffuser angle of 8 ° and 9.8 ° are 459 m/s and 270 m/s respectively. Since higher fluid flow velocity can generates lower fluid pressure, so it is confirmed that diffuser angle of 8 ° is better to be used because of providing better traction to the ground. A summary on study of different modification of diffuser is tabulated in Table 2.6 and Table 2.7.

Table 2.6: Comparison of findings of different researches (1)

Author	Analysis method	Studied model	Studied diffuser	Minimum C_D	Maximum C_D	Minimum C_L	Maximum C_L
(Hassan et al., 2014)	CFD	Figure 2.12	- 0 ° - 2.5 ° - 5.0 ° - 10.0 ° - 12.5 °	0.2517 at diffuser angle of 12.5 °	0.3233 at diffuser angle of 0°	none	none
(Moghimi & Rafee, 2018)	CFD	Figure 2.16	- 0 ° - 4.0 ° - 8.0 ° - 12.0 ° - 16.0 ° - 20.0 °	0.382 at diffuser angle of 8.0 °	0.412 at diffuser angle of 0°	-0.17 at diffuser angle of 20.0 °	0.23 at diffuser angle of 0°
(Hu et al., 2011)	CFD	Figure 2.20	- 0 ° - 3.0 ° - 6.0 ° - 9.8 ° - 12.0 °	0.2487 at diffuser angle of 6 °	0.2841 at diffuser angle of 0°	0.2586 at diffuser angle of 12.0 °	0.3350 at diffuser angle of 0°
(Sucipto & Widodo, 2018)	CFD	Figure 2.5	Number of channels in diffuser - plane diffuser - 2 channel - 3 channel - 4 channel	0.7384 at 4 channel diffuser	0.7423 at plane diffuser	-0.298 at 2 channel diffuser	-0.282 at plane diffuser

Table 2.7: Comparison of findings of different research (2)

Author	Analysis method	Studied Diffuser	Findings
(Abid et al., 2017)	CFD	Diffuser angle 14 °	Vehicle alone - Downforce 11.2 N - Drag force 109.0 N Vehicle with diffuser - Downforce 84.8 N - Drag force 115.6 N
(Huminic & Huminic, 2020)	CFD	- Plane diffuser - Curved diffuser with angle - 2 ° - 4 ° - 6 ° - 8 °	- Curved diffuser has lower C_L compared to plane diffuser (Change of C_L= 20.2%) - Curved diffuser has smaller C_D for smaller diffuser angle (2 °, 4 °)
(Sreeradh, 2018)	CFD	Diffuser angle - 7 ° - 8 ° - 9.8 °	- Highest velocity under car body at diffuser angle 8 ° (459 m/s) - Lowest pressure under car body at diffuser angle 8 °, 9.8° (4.48 bar)

CHAPTER 3
METHODOLOGY

Figure 3.1 is the flow chart for the overall process in the methodology. The process started with the CFD Fluent solver settings validation by referring to wind tunnel experiment done by Razak, (2009). CAD tool is used to recreate the simpler F1 IN SCHOOLS car model as used in the wind tunnel experiment. Fluid volume and mesh generation for the model ere followed by mesh validation before importing the mesh into CFD Fluent. After that, several solver settings will be tested for the simulations to discover which settings provide results with smallest percentage different with the result obtained from wind tunnel experiment. The selected solver settings will then be applied on the CFD simulation of the study.

For the study, 3D modelling of F1 IN SCHOOLS Car is done by using Autodesk Fusion 360. Simplification is done on the original model to create a simplified 2D midplane of the car body by eliminating components such as wheels, axle, front and rear wings. Next, the original model is simplified into a 3D car body by eliminating wheels, axle, front and rear wings. Lastly, the original model is simplified by replacing the wheel bearings with extruded cylinders. The study is then proceeded with fluid volume and mesh generation for the three models. After that, CFD simulation is done on the three models with selected solver settings. Results obtained is tabulated for further comparison and discussion. Finally, conclusion and recommendations are done based on the discussions made.

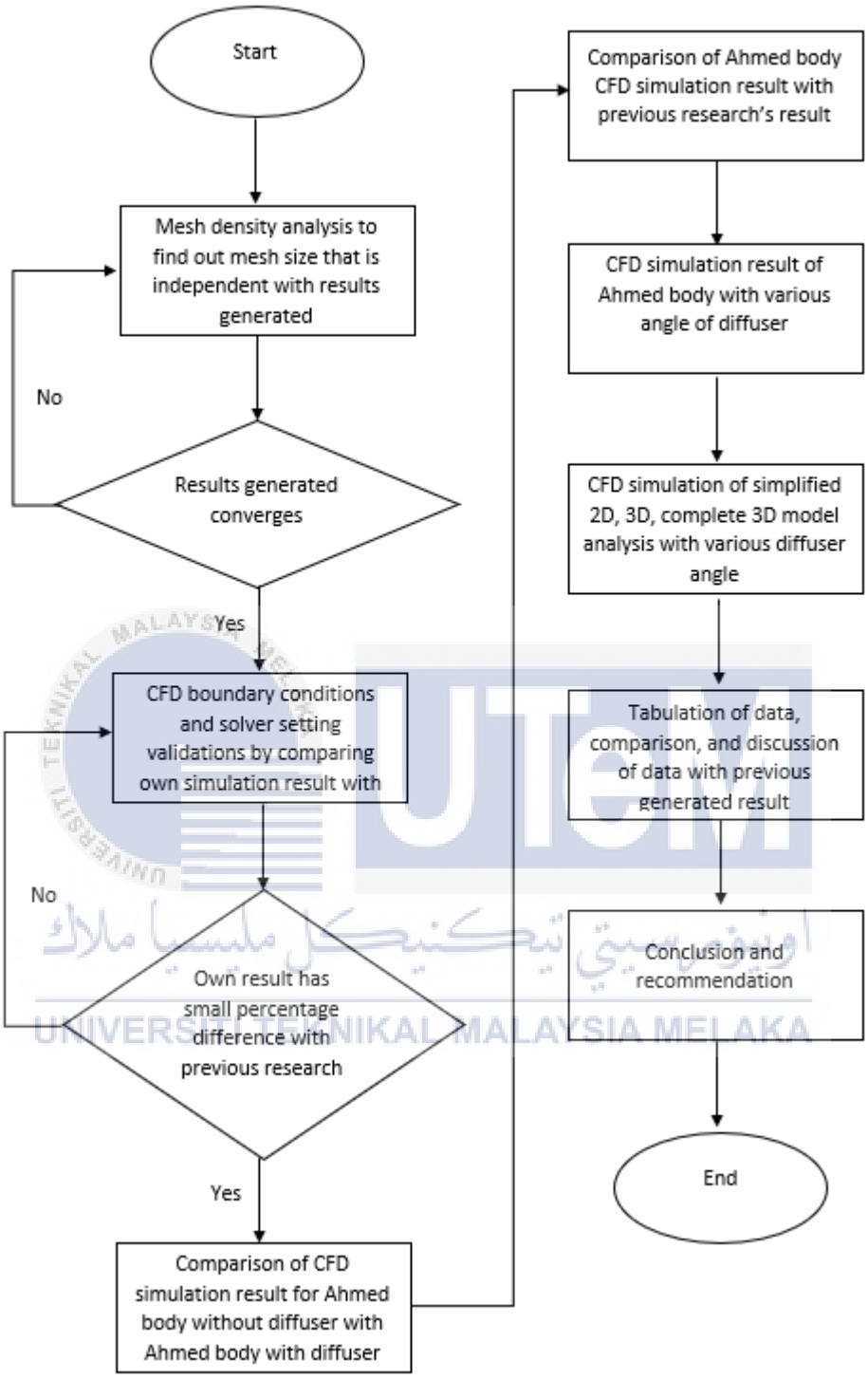

Figure 3.1: Flow Chart for Methodology

3.1 Meshing

3.1.1 Mesh density analysis

Mesh density analysis is done to ensure the accuracy of the simulation's result. The higher the mesh density, the more accurate the analysis result. However, it may take longer time for simulation process. First, the general mesh size of the fluid volume for simpler F1 IN SCHOOLS car is set to 20 mm, the car surface mesh size is set to 10 mm for CFD simulation. Then, the CFD simulation is repeated with decreasing car surface mesh size at rate of 0.5 mm until it reaches 1 mm. After that, the CFD simulation is repeated with decreasing car surface mesh size at rate of 0.1 mm until it reaches 0.5 mm. The purpose of the increasing the mesh density of the fluid volume is to make sure the simulation results of analysis are not affected by the change of mesh density. This is because the result will converge to a repeating solution at certain mesh density.

3.1.2 Mesh refinement

The type of mesh used in the study is referred to Hu et al. (2011) research, as shown in Figure 3.2. In the research, inflation layers are applied on the car's surface. Tetrahedral mesh is applied to other parts in the fluid volume. Since the important areas in the simulation are around the car's surface, mesh refinement is done closed to the car's surface to obtain a more accurate result. The element size from the car surface is set to 1 mm and increased to further part in the fluid volume at a constant rate of 1.05 until it reached a mesh size of 20 mm. For meshing in the simplified 2D analysis, the halved fluid volume of simplified 3D analysis, and the complete halved fluid volume of the complete 3D model, the mesh applied will be the same as discussed above. Table 3.1 shows the mesh settings for simulation of simpler F1 IN SCHOOLS model while the unmentioned settings is remained as default by system.

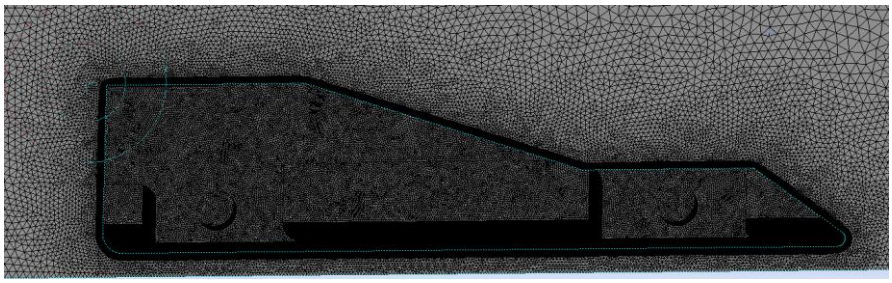

Figure 3.2: Inflation layers mesh on the simplified car body

Table 3.1: Mesh settings for simulation of simpler F1 IN SCHOOLS car model.

Mesh detail	Setting
Element size	20.0 mm
Sizing growth rate	1.05
Smoothing quality	High
Model's face sizing	1.0 mm
Inflation layers applied on model's surface	20
Inflation layers growth rate	1.05

3.1.3 Mesh validation

Mesh validation can be done by checking the skewness and orthogonal quality of the mesh. Mesh with a skewness value closed to zero is considered excellent. However, the skewness value within the benchmark is also acceptable. For triangular and tetrahedral mesh, the skewness value should be kept under 0.95 and orthogonal quality for the mesh must be in-between 0.1 to 1. If the mesh quality is not within the acceptable range, adjustment on mesh settings will be done. This is to ensure the reliability of the results generated using the mesh. The most common ways to reduce the skewness value are selecting the suitable mesh type at the part with complex geometry, setting smaller element size, or applying smaller element size for the part with complex geometry.

3.2 Validation of CFD Boundary Conditions and Solver Settings

The study is started with validation of CFD boundary conditions and solver settings. It is validated by referring to previous research of Razak, (2009). In the study, wind tunnel result of a simpler F1 IN SCHOOLS car model (Figure 3.3) is compared with the CFD result to check which solver settings able to obtain results closest to the wind tunnel experiment result. Then, percentage difference of lift and drag coefficient is evaluated. The experiment is repeated with different inlet velocity starting from 20 m/s to 32 m/s. The boundary conditions applied on the fluid volume as shown in Table 3.2, referred to research done by Hu et al. (2011). The fluid type of fluid volume is set as air as the competition is held in an open area in a closed room. The midface of the fluid volume is set as slip symmetry for the computation recognise it as symmetry plane. Outlet pressure is set to zero so that no interruption of airflow at the back of the car. The unmodified faces of fluid volume will remain as walls. The fluid volume created is shown in Figure 3.4 and it is halved to decrease computation resources. Result validation can be done by conducting the convergence study of results. The absolute criteria under solution's monitor residual for continuity, x-velocity, y-velocity, z-velocity and turbulent kinetic energy is set to 1x10^-5 for the convergence conditions of results.

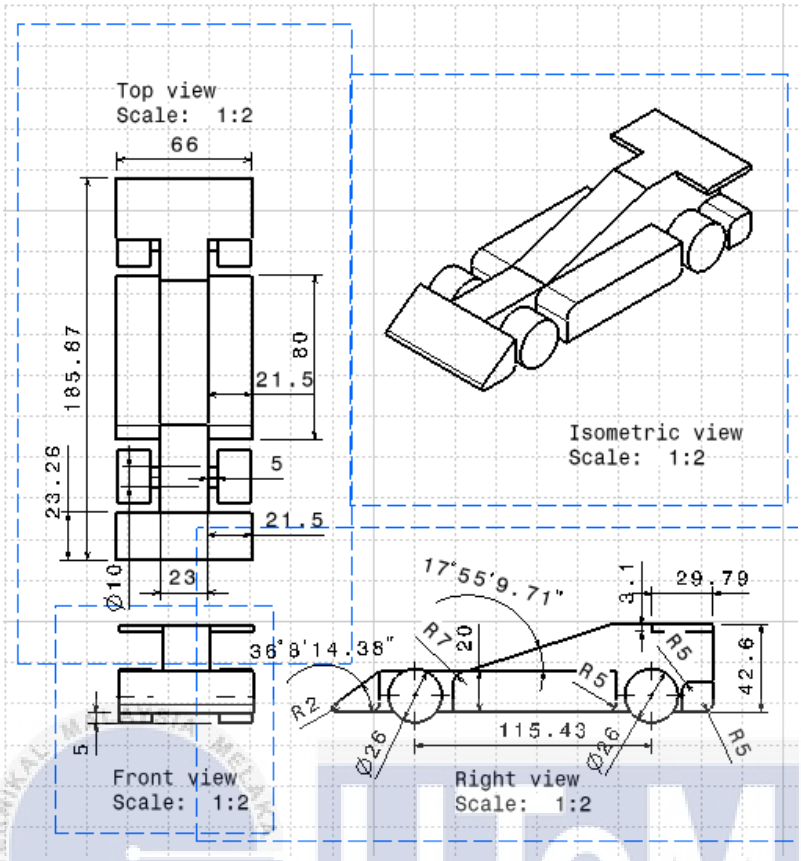

Figure 3.3: Drawing of F1 I SCHOOLS car model (Razak, 2009)

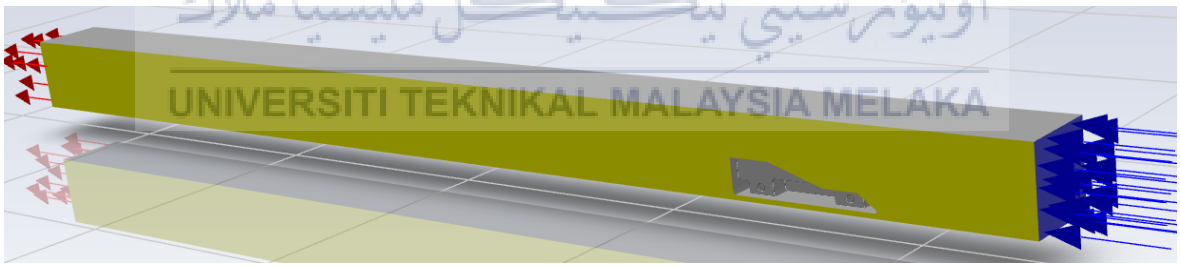

Figure 3.4: Fluid volume for CFD solver validation

Table 3.2: Boundary conditions for fluid volume

Region	Boundary Conditions
Fluid type	Air
Front face (inlet)	Velocity = 20 m/s
Mid face	Slip symmetry
Back face (outlet)	Pressure = 0 Pa

The solver setting for the CFD simulation is shown in Table 3.3. The simulation's solver type is pressure-based and time is set to steady for the simulation. Turbulent model applied for the simulation is the Realizable k-epsilon model. The turbulent model provides excellent performance for flow involving rotation and boundary layers, which is suitable for simulating flow behaviour of complex structures. For solution method, scheme is set to Coupled while spatial discretization of gradient is set to least squares cell based. Pressure, momentum, turbulent kinetic energy, and turbulent dissipation rate is set to second order to obtain more accurate result. The validated CFD solver settings will then be used for CFD simulation of 2D and 3D simplified model and complete 3D model.

Table 3.3*: Solver settings for CFD simulation*

Type	Setting
Solver type	Pressure-Based
Turbulent model	Realizable k-epsilon model
Scheme	Coupled
Gradient	Least Square Cell Based
Pressure	Second Order
Momentum	Second Order Upwind
Turbulent Kinetic Energy	Second Order Upwind
Specific Dissipation Rate	Second Order Upwind

3.3 Ahmed Body CFD Simulation

Ahmed body CFD simulation is done to compare own CFD simulation result with previous CFD simulation result done by Meile et al., (2011). First of all, 3D model of Ahmed body is build according to dimensions stated by Meile et al., (2011) using design modeller with proper enclosure of fluid volume and it is halved at the symmetry plane to save computation resources. Then, result of coefficient of drag is tabulated for percentage differences evaluation. The simulation follows the range of inlet velocity set by the previous simulation which starts from 3 m/s and ends with 70 m/s. After that, the simulation is repeated with the same range of inlet velocities but with the presence of diffuser. The diffuser on the Ahmed body has a constant length of 150 mm and angle of 15 degree for the purpose of identifying the influence of diffuser on aerodynamic behaviour of Ahmed body. Then, the difference of coefficient of drag is evaluated. Lastly, simulation of Ahmed body with various diffuser angle is conducted at constant inlet velocity of 70 m/s to study the effect of various diffuser angle towards the drag and lift coefficient.

3.4 3D Modelling of F1 IN SCHOOLS Car Model

Figure 3.5 shown the part name of F1 IN SCHOOLS Car model. The modelling of F1 IN SCHOOLS Car is done using Autodesk Fusion 360. Features used to model the car is as shown in Table 3.4. Fillet is also done on the model for smoother airflow. Car body (lower) is extruded on the right side first then mirrored at the midplane to become a complete car body (lower).

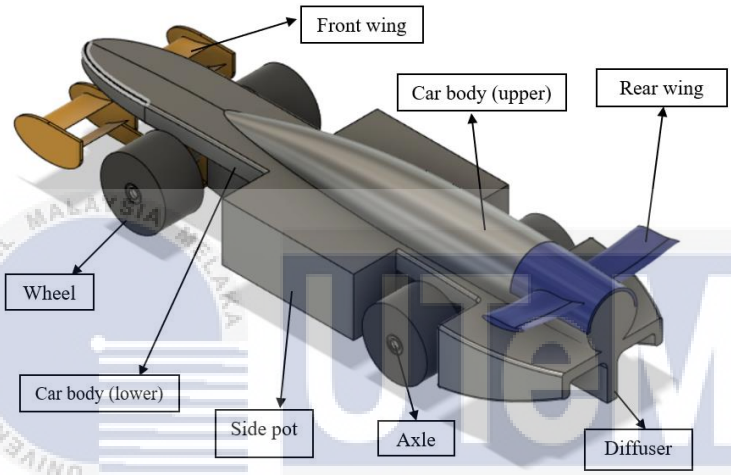

Figure 3.5: Part name of F1 IN SCHOOLS Car model.

Table 3.4 Feature used in Autodesk Fusion 360 to create part.

Part name	Feature used
Car body (lower)	- Sketches done as shown in Figure 3.6. - Extruded as shown in Figure 3.7.
Side pot & diffuser	- Sketches done as shown in Figure 3.8. - Extruded as shown in Figure 3.9.
Front wing	- Sketches done on different planes. - Extruded and mirrored as shown in Figure 3.10.
Car body (upper)	- Free form cylinder surface created and edited as shown in Figure 3.11 - Patched and stitched to create solid. - Combined with car body (lower) as one body

Rear wing	- Sketches done on different planes. - Support extruded. - Free form surface extruded and edited as shown in Figure 3.12. - Patched and stitched to create solid then combined with support to become one body. - Subtract from car body as tool but tool kept.
Wheel	- Imported from other resources.
Axle	- Imported from other resources.
Whole body assembly	- Car body is grounded. - Rigid joint applied to front and rear wing with car body. - Revolute joint applied to wheels and axles

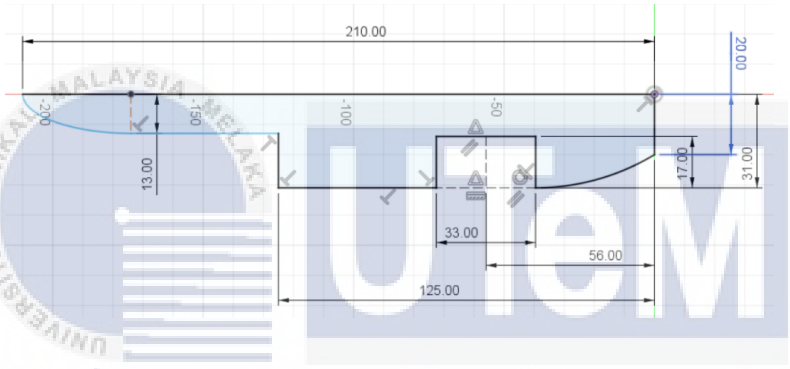

Figure 3.6: Car body (lower) sketches.

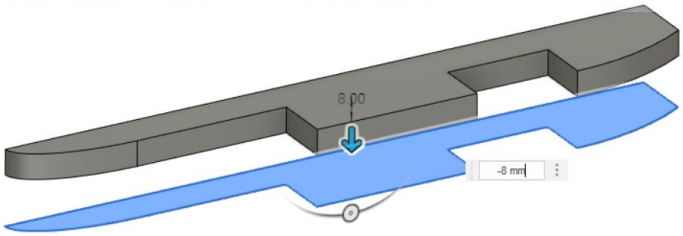

Figure 3.7*: Car body (lower) extrude.*

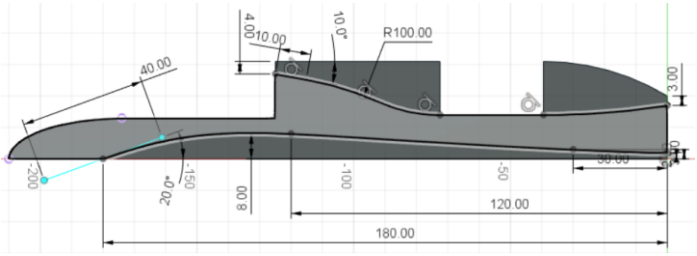

Figure 3.8*: Air flow channel sketches.*

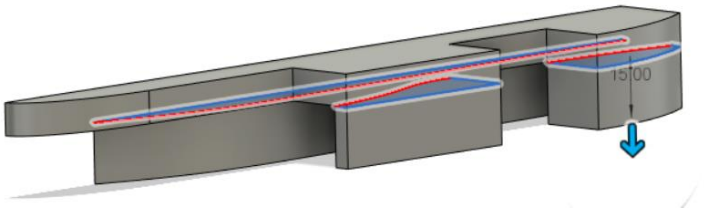

Figure 3.9*: Air channel extrude.*

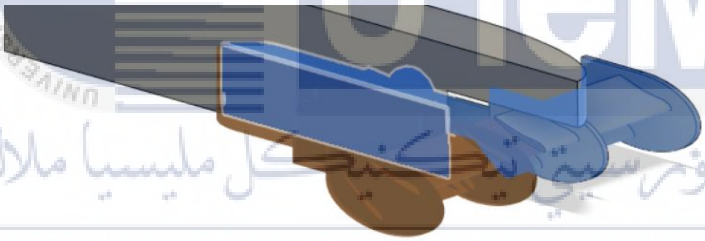

Figure 3.10*: Front wing mirrored.*

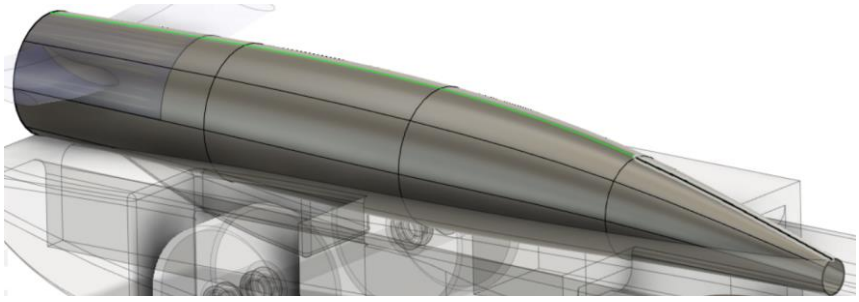

Figure 3.11: Free form surface of car body (upper)

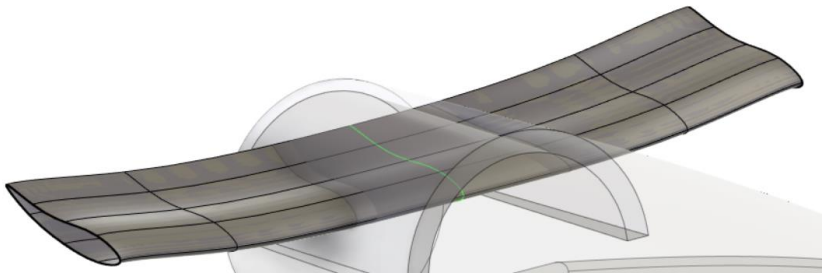

Figure 3.12: Free form surface of rear wing

3.5 CFD Simulation

3.5.1 Simplification of model

The model needed to be simplified first before sending it to Ansys Fluent using Autodesk Fusion 360. Simplification is done by removing unnecessary components such as free form planes and wheel bearings and this simplification is done on the complete model of F1 IN SCHOOLS Car. This will remove the components that are not required for the simulation. Besides, meshing of the model can also be done more easily as meshing for relatively small wheel bearings required specific settings. Then, the gap in-between the wheels and axles are filled with extruded cylinder as shown in Figure 3.13 (a), preventing the empty gap from interrupting the airflow around the wheels. All components in the design are then combined into one body to simplify the creation of fluid volume. Rectangular fluid volume is then created surrounding the car body as a medium of airflow. The fluid volume surface is offset from the car body because walls close to the car body will interrupt and limit the airflow surrounding the car. The side surfaces of the fluid volume were offset to one car length, front surface is offset to one car length while rear surface is offset to seven car length following the research done by (Paturrahman et al., 2018). Car body is then removed from the fluid volume is shown in Figure 3.13 (b). Since the car body is symmetrical at the midplane, the simulation can be conducted by halving the fluid volume at the midplane as shown in Figure 3.13 (c) as the airflow on both sides is assumed to be identical. However, due to the difficulty of applying mesh on parts with complex geometry such as wheels and wings, the analysis will be done on simplified 2D midplane and simplified 3D car body first

which will be discussed in section 3.4 Simplified 2D Model Analysis and 3.5 Simplified 3D Model Analysis. We will then analyse the airflow of complete 3D model which includes all the components shown in Figure 3.13 (c).

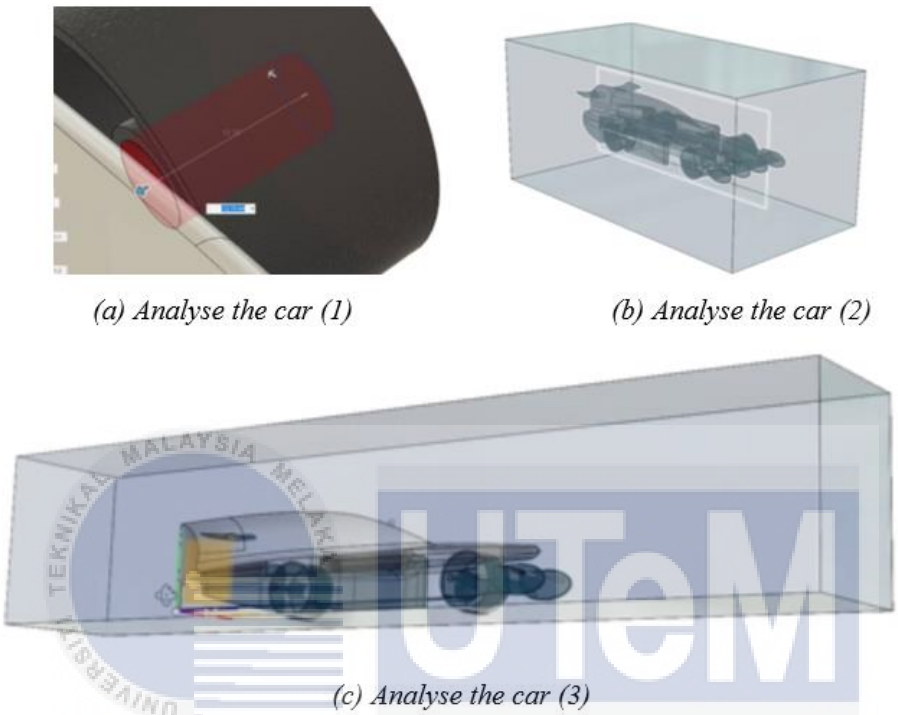

(a) Analyse the car (1)

(b) Analyse the car (2)

(c) Analyse the car (3)

Figure 3.13: (a) Analyse the car (1); (b) Analyse the car (2); (c) Analyse the car (3)

3.5.2 Simplified 2D Model Analysis

The first analysis is done by using a simplified 2D midplane of the car body. Simplification is done by neglecting the wheels, axles, front and rear wings on the car. This is to keep the simulation time to the shortest time possible and save computer resources. Then, car body's midplane is simplified using Autodesk Fusion 360, as shown in Figure 3.14, followed by creating the fluid volume with an offset distance of front and rear walls as stated in section 3.4.1. Boundary conditions and solver settings will also be following the settings discussed in section 3.2. The analysis is conducted with the ground clearance greater than the absolute minimum distance of 1.5 mm as stated by F1 In Schools (2020) in the technical regulation of F1 IN SCHOOLS competition handout. Next, the analysis is started by simulating the airflow behaviour at diffuser angle of 0 ° followed by increasing diffuser angle with the rate of two degrees to diffuser angle of 20 °, referred from the research of Moghimi & Rafee, (2018). For each simulation with different diffuser angles, mesh validation is done to ensure better mesh quality. Then, the result of the airflow velocity and the surrounding air pressure behaviour is recorded for analysis. The coefficient of drag and lift is then tabulated for further evaluation. However, there is limitation of 2D analysis as the 2D simplified plane cannot capture the airflow behaviour entering the bottom of the car body from both sides. Hence, the result is less reliable.

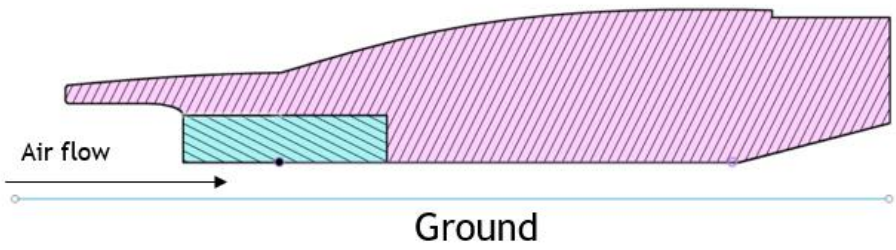

Figure 3.14: Simplified midplane of car body.

3.5.3 Simplified 3D Model Analysis

The next analysis is then conducted by using a simplified 3D car body. Simplification done is similar with previous 2D analysis where the wheels, axles, front wing and rear wings on the car are removed. Then, the fluid volume is created with offset of front and rear walls as stated in section 3.4.1, and it is halved at the midplane for simulation, as shown in Figure 3.15. Boundary conditions and solver settings will also be using the same settings, as stated in section 3.2.2. The ground clearance is set to a distance greater than the absolute minimum distance of 1.5 mm, as stated by F1 In Schools (2020) in the technical regulation of F1 IN SCHOOLS competition handout. Next, the studied diffuser angle is also the same as the previous analysis. It is started by diffuser angle of 0 °, followed by increasing diffuser angle with the rate of two degrees to diffuser angle of 20 °, referred from Moghimi & Rafee's (2018) research. For each simulation with a different diffuser angle, mesh validation is done to ensure better mesh. Record of airflow velocity and behaviour of air pressure around the car body is done for further analysis. Tabulation of the coefficient of drag and lift is also done for further evaluation. This time, airflow entering from the side into the bottom of car and airflow closed to the curved surface can be evaluated.

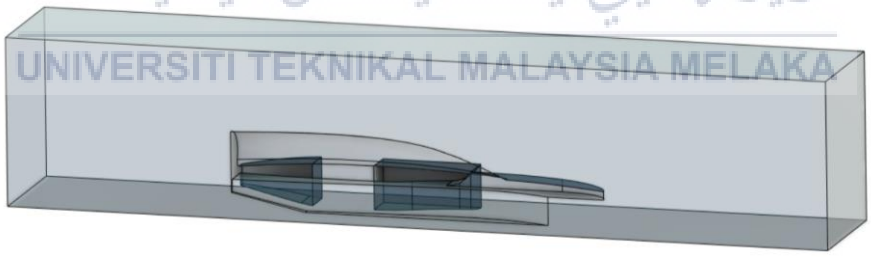

Figure 3.15: Fluid volume of simplified 3D car body

3.5.4 Complete 3D Model Analysis

To obtain a more accurate airflow behaviour around the car body, airflow analysis on the complete 3D model needed to be done. The simplification of the model and fluid

volume creation is discussed in section 3.4.1, where the free form plane is removed, wheel bearings are replaced with extruded cylinders, and fluid volume is created with offset of walls and halved at the midplane and both front and rear wings were adjusted to simple shape without tilt angle. Then, the airflow simulation is run with different a diffuser angle starting from 0 ° to 20 ° with a constantly increasing rate of two degrees, referred to research done by Moghimi & Rafee, (2018). Mesh validations are also done for each simulation of different diffuser angle. Record of airflow velocity and air pressure behaviour around the car body is done for further analysis. The tabulation of drag and lift coefficient is also done for further evaluation. After that, all the results obtained are compared and discussed for topic discussion and conclusion. Then, the sidepot of complete 3D model is removed by filling with solid using CAD software and CFD simulation is conducted to compare the effect of existence of sidepot.

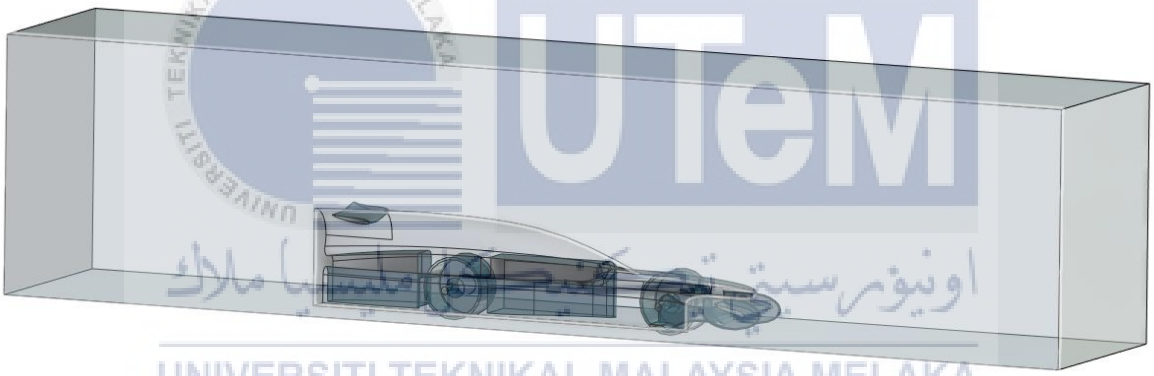

Figure 3.16: Fluid volume of complete 3D car body

CHAPTER 4
RESULT AND DISCUSSION

4.1 Mesh Density Analysis Using Simpler F1 IN SCHOOLS Car Model.

Table 4.1 shows the result of mesh density analysis using the simpler F1 IN SCHOOLS car model. The inlet velocity is fix at 25 m/s for the simulations with different surface element size. As shown in the table, the results of drag and lift coefficient converged to a constant value when the surface element size equals to 1 mm or the number of nodes in the mesh reached 859k. At this point, the simulation result is said to be independent of the density of mesh. Further increasing the mesh density of the mesh will not make changes to the result. According to Figure 4.1 and Figure 4.2, both drag and lift coefficient have unsteady values when number of nodes smaller than 500000. However, at number of nodes close to 1000000, the graph converges steadily. Thus, surface element size of 1 mm is selected to be used for further simulation as it provides simulation result that is independent of the mesh density. The analysis is continued until surface element size of 0.5 mm to make sure the converging of the graph is steady.

Table 4.1:Result of Mesh Density Analysis

surface element size (mm)	number of nodes	drag coefficient	lift coefficient
10.0	29278	1.08	-0.56
9.5	32286	1.11	-0.59
9.0	35483	1.1	-0.62
8.5	40469	1.04	-0.56
8.0	40395	1.04	-0.53
7.5	51342	1.05	-0.51
7.0	57414	1.05	-0.48
6.5	64945	1.04	-0.47
6.0	73394	1.05	-0.47
5.5	84609	1.04	-0.44
5.0	97171	1.09	-0.43
4.5	114350	1.07	-0.44
4.0	134608	1.08	-0.46
3.5	158203	1.06	-0.45
3.0	191367	1.06	-0.46
2.5	238222	1.05	-0.39
2.0	316360	1.05	-0.39
1.5	452970	1.06	-0.35
1.0	859125	1.07	-0.33
0.9	1028455	1.07	-0.33
0.8	1274830	1.07	-0.34
0.7	1633423	1.07	-0.34
0.6	2175619	1.07	-0.33
0.5	3123977	1.07	-0.33

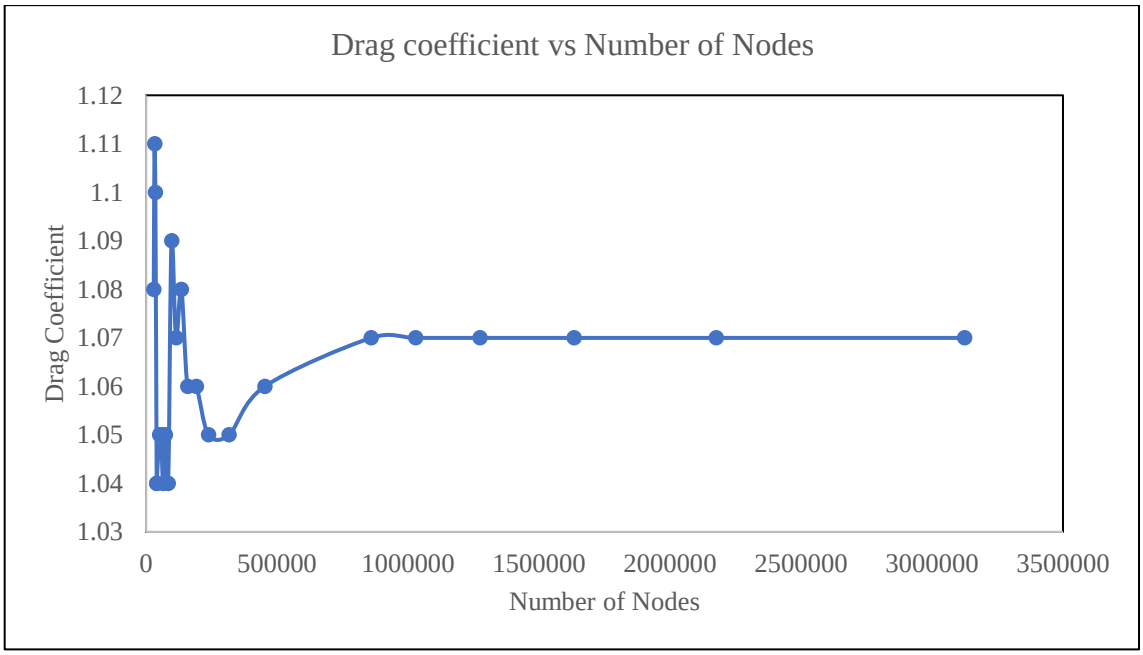

Figure 4.1: Graph of drag coefficient vs number of nodes.

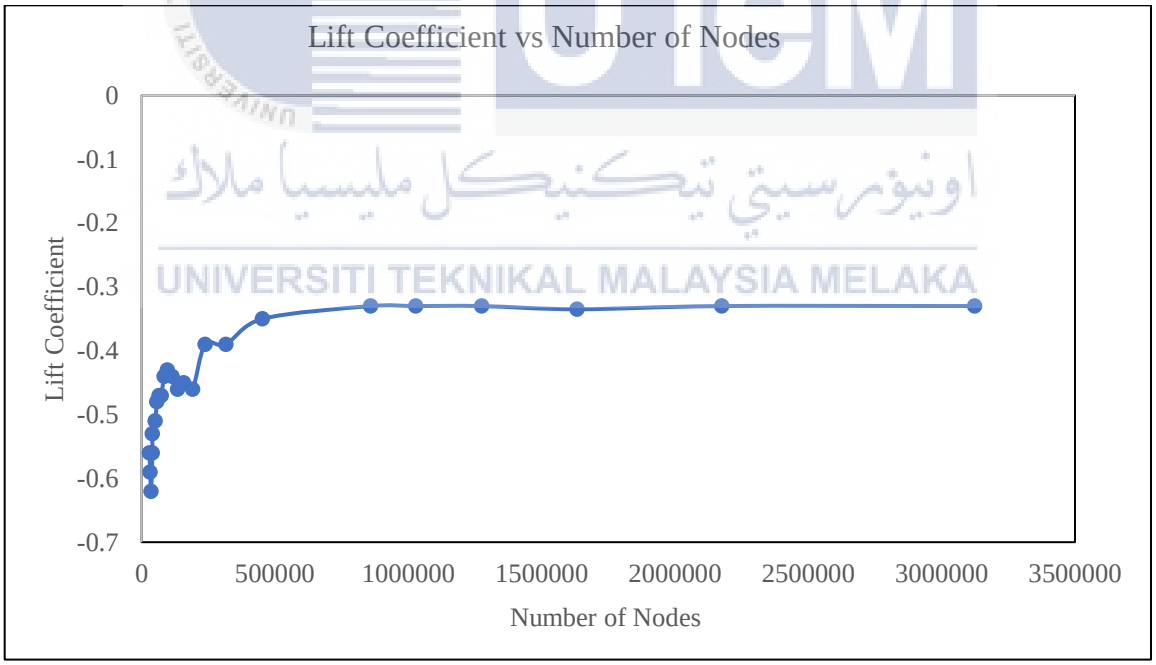

Figure 4.2: Graph of lift coefficient vs number of nodes.

4.2 Comparison of CFD simulation result

In this section, a few comparisons on the CFD simulation result will be discussed. The first comparison is by comparing the wind tunnel test result done by Razak, (2009) and own CFD simulation result with the same simpler F1 IN SCHOOLS car model. This done to verify fluent solver setting used for simulation has low percentage difference and can be used for further simulation in this study. The next is comparison of previous research of Ahmed body wind tunnel test result with own CFD simulation result to check the percentage difference of results generated, following by the comparison of simulation result of original Ahmed body and Ahmed body with diffuser to check the effect on the changes of drag coefficient. Then, comparison of various diffuser angle on Ahmed body is conducted to check which angle provides the lowest drag coefficient and suitable lift coefficient.

4.2.1 Wind Tunnel Test Result vs CFD Simulation Result

Table 4.2 and Figure 4.3 show the result of drag coefficient between wind tunnel test and CFD simulation of simpler F1 IN SCHOOLS car model. The wind tunnel test result is obtained from the previous thesis done by Razak, (2009). The smallest percentage difference happens at inlet velocity of 21 m/s where the percentage difference between the wind tunnel test result and simulation result is 0.037 % while the largest percentage difference is 9.975%, happens at inlet velocity of 32 m/s. According to Figure 4.3, both wind tunnel test and CFD simulation result for drag coefficient seems to have increasing trend as the value of inlet velocity increases. However, the result of wind tunnel test is not increase steadily which may be because of poor flow quality in the test section or noisy operation.

Table 4.2: Percentage difference of drag coefficient between wind tunnel test and CFD simulation of simpler F1 IN SCHOOLS car model.

	Drag Force (N)		Drag Coefficient		Percentage difference for drag coefficient (%)
Inlet velocity (m/s)	Wind tunnel test	CFD simulation	Wind tunnel test	CFD simulation	
20	0.284	0.2840	1.06	1.0702	0.962
21	0.313	0.3132	1.07	1.0704	0.037
22	0.350	0.3470	1.09	1.0800	0.917
23	0.372	0.3758	1.06	1.0707	1.009
24	0.428	0.4090	1.12	1.0707	4.402
25	0.469	0.4440	1.13	1.0710	5.221
26	0.507	0.4802	1.13	1.0710	5.221
27	0.556	0.5180	1.15	1.0710	6.870
28	0.598	0.5570	1.15	1.0712	6.852
29	0.641	0.5978	1.15	1.0714	6.835
30	0.675	0.6403	1.13	1.0724	5.097
31	0.752	0.6857	1.18	1.0756	8.847
32	0.815	0.7339	1.20	1.0803	9.975

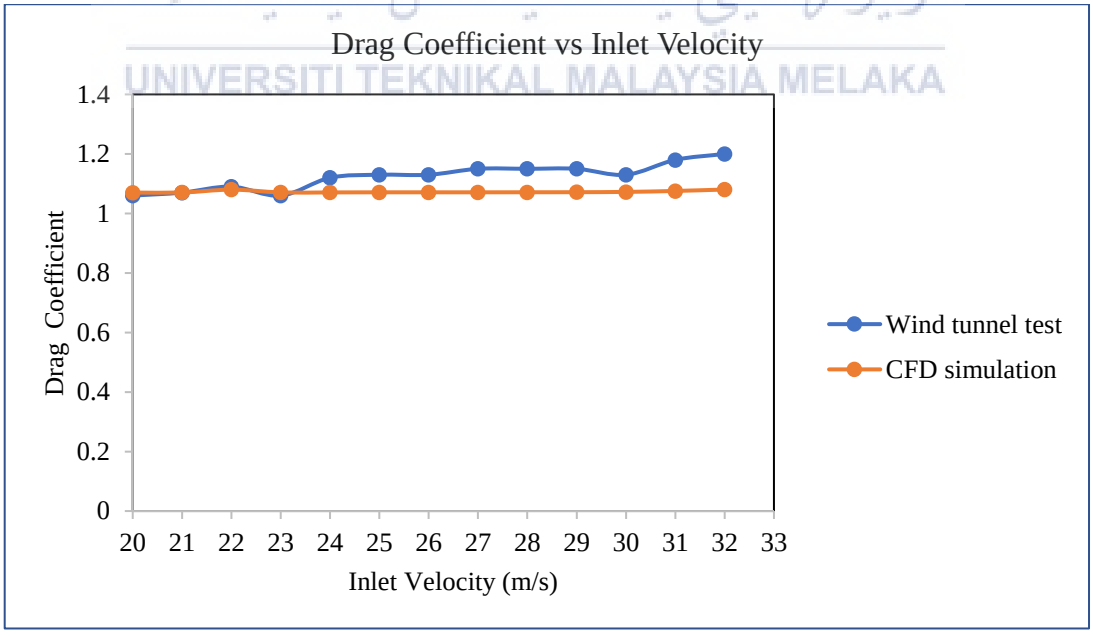

Figure 4.3: Graph of Drag Coefficient vs Inlet Velocity between wind tunnel test and CFD simulation of simpler F1 IN SCHOOLS car model.

Table 4.3 and Figure 4.4 show the results of lift coefficient between wind tunnel test and CFD simulation of simpler F1 IN SCHOOLS car model. The smallest percentage difference among the result happens at inlet velocity of 25 m/s where the percentage difference between the wind tunnel test result and simulation result is 0.789 % while the largest percentage difference is 20.963% happens at inlet velocity of 32 m/s. According to Figure 4.4, both wind tunnel test and CFD simulation result for drag coefficient seems to have decreasing trend as the value of inlet velocity increases and the same situation happen where the result of wind tunnel test is not decrease steadily which may be because of poor flow quality in the test section or noisy operation.

Table 4.3: Percentage difference of lift coefficient between wind tunnel test and CFD simulation of simpler F1 IN SCHOOLS car model.

	Lift Force (N)		Lift Coefficient		Percentage difference for lift coefficient (%)
Inlet velocity (m/s)	Wind tunnel test	CFD simulation	Wind tunnel test	CFD simulation	
20	-0.096	-0.0874	-0.36	-0.3290	8.611
21	-0.108	-0.0995	-0.37	-0.3401	8.108
22	-0.112	-0.1140	-0.35	-0.3540	1.143
23	-0.113	-0.1260	-0.35	-0.3590	2.857
24	-0.145	-0.1408	-0.38	-0.3680	3.158
25	-0.158	-0.1560	-0.38	-0.3770	0.789
26	-0.170	-0.1730	-0.38	-0.3850	1.316
27	-0.203	-0.1901	-0.42	-0.3930	6.429
28	-0.218	-0.2080	-0.42	-0.4004	4.667
29	-0.240	-0.3800	-0.43	-0.4073	5.279
30	-0.263	-0.2476	-0.44	-0.4147	5.750
31	-0.300	-0.2688	-0.47	-0.4216	10.298
32	-0.367	-0.2899	-0.54	-0.4268	20.963

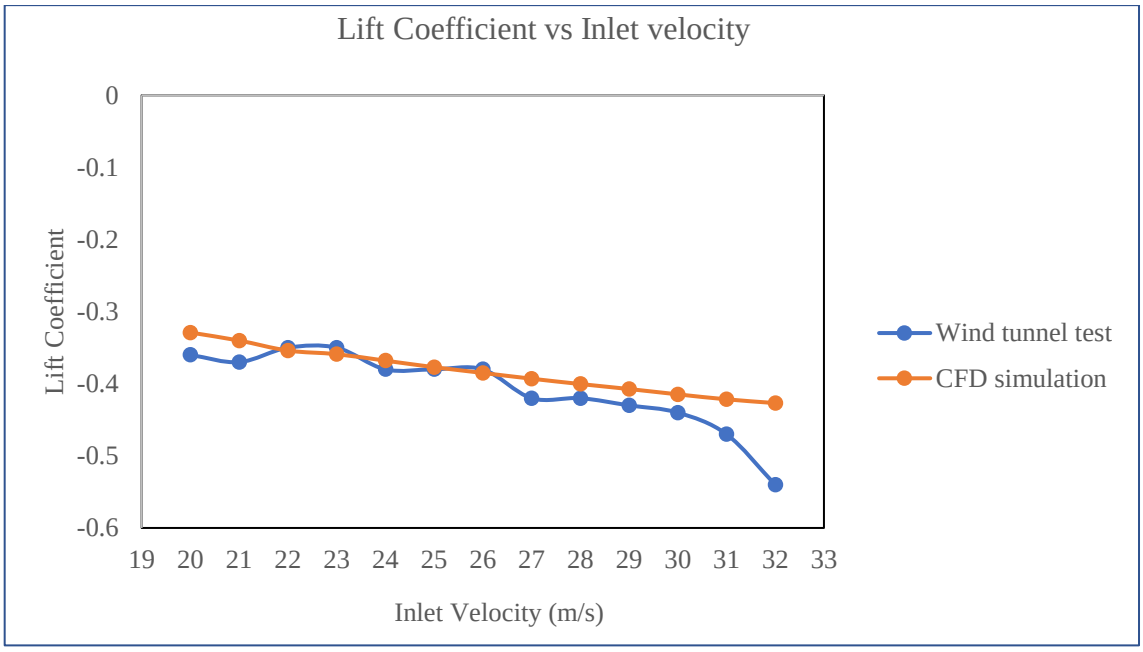

Figure 4.4: Graph of Lift Coefficient vs Inlet Velocity between wind tunnel test and CFD simulation of simpler F1 IN SCHOOLS car model.

Figure 4.5 shows the velocity pathline at simulation result of inlet velocity of 25 m/s. The blue pathline indicates that there is zero velocity at the rear part of the moving car body. This caused vacumm at the rear part of the car and created suction force which drags the car from moving forward.

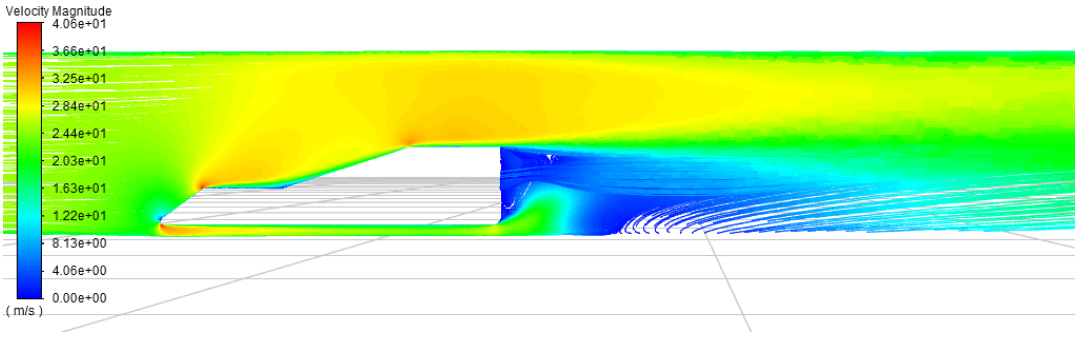

Figure 4.5: Velocity pathline of simplified F1 IN SCHOOL car model at inlet velocity of 25 m/s.

4.2.2 Ahmed body CFD simulation result comparison

Table 4.4 and Figure 4.6 shows the comparison of Ahmed body CFD simulation result with previous study's result done by Meile et al., (2011). Based on the result, both simulation results show decreasing trend in drag coefficient. According to Figure 4.6, the coefficient of drag for CFD simulation decreases drastically starting from 0.39309 to 0.32225 until it reaches the inlet velocity of 10 m/s. After that, the drag coefficient decreases slowly starting from inlet velocity of 10 m/s to 70 m/s. For the simulation result done by Meile et al., (2011), the drag coefficient decreases gradually from 0.36001 to 0.28445 throughout the tested inlet velocity. For the overall result comparison, the highest percentage difference is 9.189 % which occurs at inlet velocity of 3 m/s and lowest percentage difference is 0.564 % at inlet velocity of 30 m/s. The occur of drag force is explained by stagnation of pressure at the front part of Ahmed body and lower pressure zone at the rear part of Ahmed body at high speed which can be seen in Figure 4.7. This will slow down the body from moving forward.

Table 4.4: Comparison of Ahmed body CFD simulation result with previous study's result

Inlet velocity (m/s)	C_D, CFD simulation	C_D, (Meile et al., 2011)	Percent Difference (%)
3	0.39309	0.36001	9.189
4	0.36666	0.35684	2.753
5	0.35029	0.35380	0.990
6	0.33728	0.35088	3.874
7.5	0.32807	0.34670	5.372
10	0.32225	0.34027	5.293
15	0.31625	0.32919	3.929
20	0.31243	0.32010	2.395
30	0.30828	0.30655	0.564
40	0.30649	0.29744	3.042
50	0.30489	0.29133	4.655
60	0.30388	0.28722	5.801
70	0.30311	0.28445	6.559

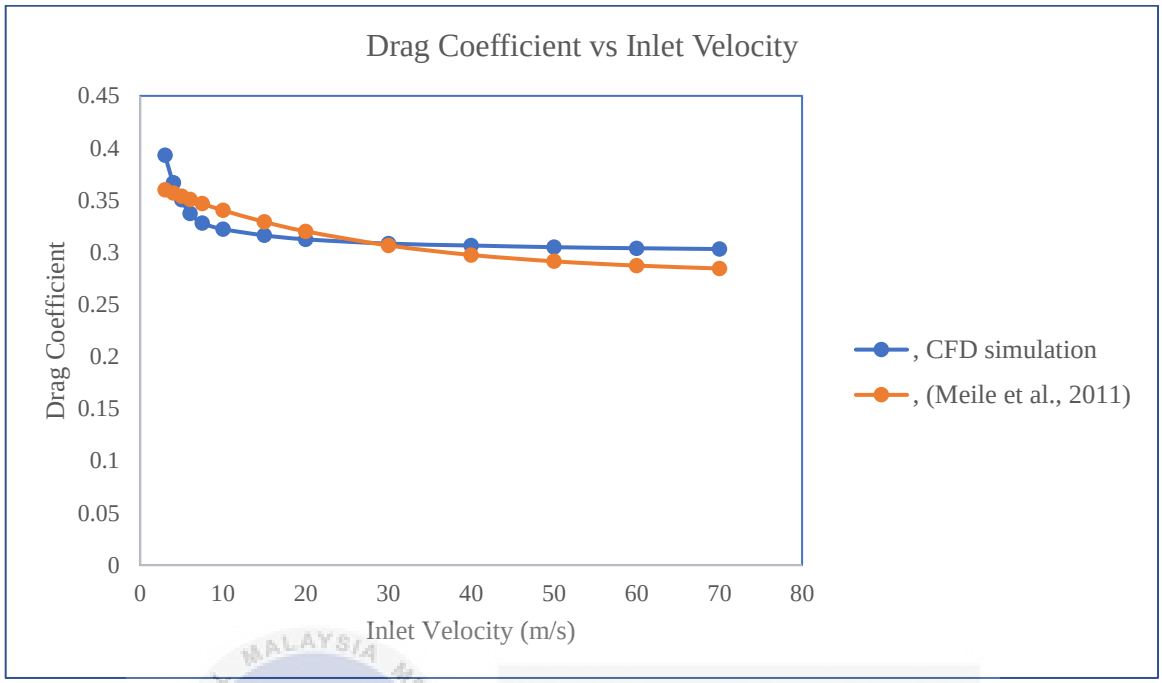

Figure 4.6: Graph of Drag Coefficient vs Inlet velocity of Comparison of Ahmed body CFD simulation result with previous study's result.

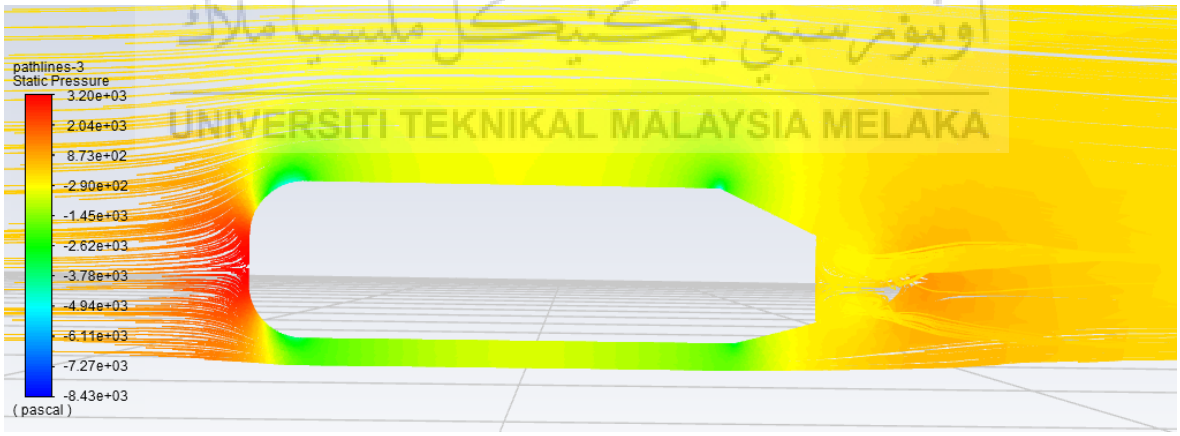

Figure 4.7: Pressure pathline of Ahmed body with diffuser at inlet velocity of 70 m/s

4.2.3 Ahmed body with diffuser CFD simulation result

Table 4.5 and Figure 4.8 show the comparison of Ahmed body simulation result with simulation result of Ahmed body with constant diffuser angle of 15 ° and constant diffuser length of 150 mm. According to Figure 4.8, the overall drag coefficient of the Ahmed body with diffuser has lower drag coefficient compared to the original Ahmed body. The percentage difference of the simulation result increases with the increase of inlet velocity. The difference of Ahmed body with diffuser and without diffuser can be seen by comparing the results shown in Figure 4.9 and Figure 4.10. The vacuum area at the rear part of original Ahmed body has bigger area compared to vacuum area at the rear part of Ahmed body with diffuser. This cause smaller drag force on the Ahmed body with diffuser due to smaller suction force which drags the body from moving forward. Besides, the higher the inlet velocity, the greater the effect of diffuser in reducing the drag coeffficient which is shown in Table 4.5.

Table 4.5: Ahmed body CFD simulation result (with diffuser and without diffuser).

Inlet velocity (m/s)	C_D with diffuser	C_D without diffuser	Percent Difference (%)
3	0.35492	0.39309	9.710
4	0.32844	0.36666	10.424
5	0.31266	0.35029	10.743
6	0.30036	0.33728	10.946
7.5	0.29017	0.32807	11.552
10	0.28520	0.32225	11.497
15	0.27913	0.31625	11.737
20	0.27564	0.31243	11.775
30	0.27100	0.30828	12.093
40	0.26816	0.30649	12.506
50	0.26625	0.30489	12.673
60	0.26461	0.30388	12.923
70	0.26354	0.30311	13.055

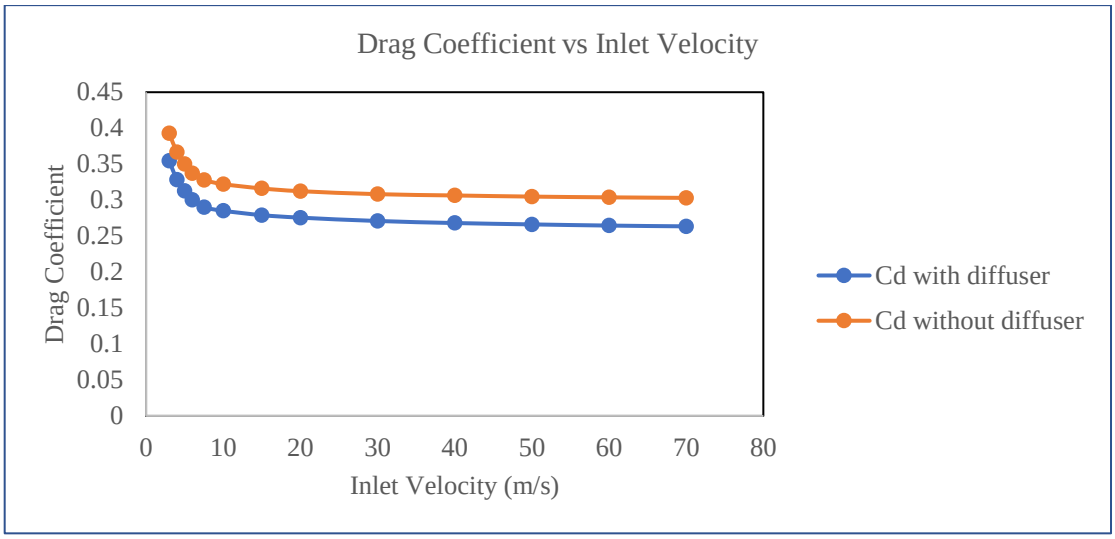

Figure 4.8: Graph of Drag Coefficient vs Inlet Velocity for Ahmed body CFD simulation result (with diffuser and without diffuser)

Figure 4.9: Velocity pathline of Ahmed body without diffuser at inlet velocity of 70 m/s

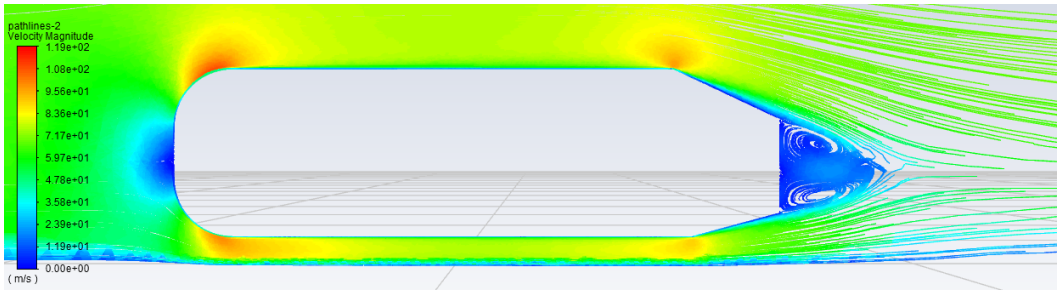

Figure 4.10: Velocity pathline of Ahmed body with diffuser at inlet velocity of 70 m/s

4.2.4 Ahmed body with various diffuser angle CFD simulation result

Table 4.6, Figure 4.11 and Figure 4.12 show the CFD simulation results of various diffuser angle towards the drag coefficient and lift coefficient of Ahmed body at a constant inlet velocity of 70 m/s. Based on Figure 4.11, the drag coefficient of Ahmed body decreases with the increasing of diffuser angle. However, there is a slight raise in drag coefficient at diffuser angle of 12 ° and 16 ° due to the present of flow separation zone generated at the diffuser part as shown in Figure 4.13. The vortices generated at the diffuser has caused vacuum thus increases the drag force. The decrease of overall drag coefficient is due to redirect of air flow by diffuser into the vacuum zone at the rear part of body. The optimum diffuser angle which generates lowest drag coefficient is at diffuser angle of 10 °.

For the lift coefficient, the lift coefficient of Ahmed body decreases gradually as the diffuser angle increases. This is because the air velocity at the trailing edge of diffuser increases as the diffuser angle increases which can be seen in Figure 4.9 and Figure 4.10. By comparing the air velocity at the edge of diffuser, Ahmed body with diffuser has higher air velocity at the bottom of body. This causes the air flow velocity at the bottom of Ahmed body increases thus creating lower pressure which decreases the lift coefficient. Starting at diffuser angle of 12 °, the value of lift coefficient has become negative which the Ahmed body starts to experience downforce.

Table 4.6: CFD simulation result of Ahmed body with various diffuser angle.

diffuser angle (°)	drag coefficient	lift coefficient
0	0.3028	0.3332
2	0.2859	0.2624
4	0.2779	0.2012
6	0.2706	0.1409
8	0.2637	0.0768
10	0.2594	0.0104
12	0.2680	-0.0376
14	0.2631	-0.0969
16	0.2641	-0.1379
18	0.2628	-0.1985
20	0.2617	-0.2169

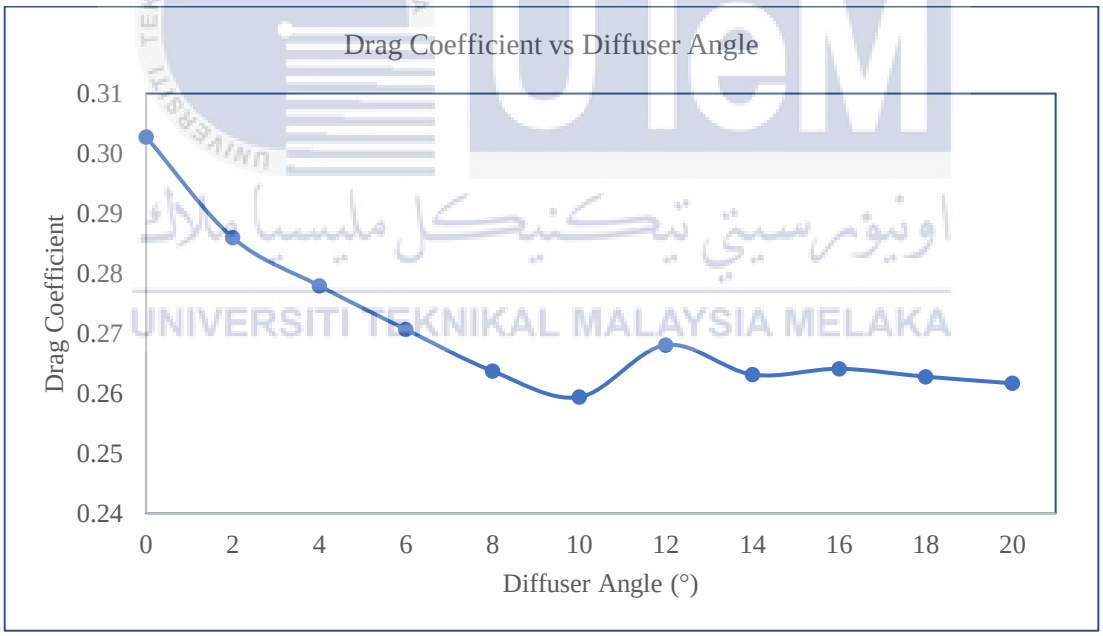

Figure 4.11: Graph of drag coefficient vs diffuser angle of Ahmed body with various diffuser angle.

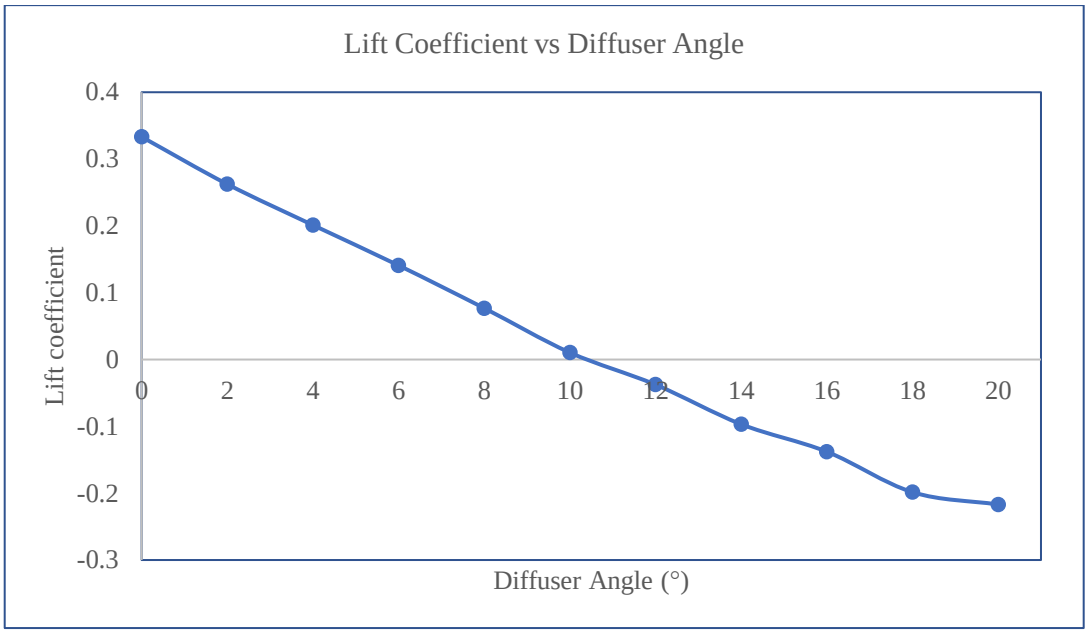

Figure 4.12: Graph of lift coefficient vs diffuser angle of Ahmed body with various diffuser angle.

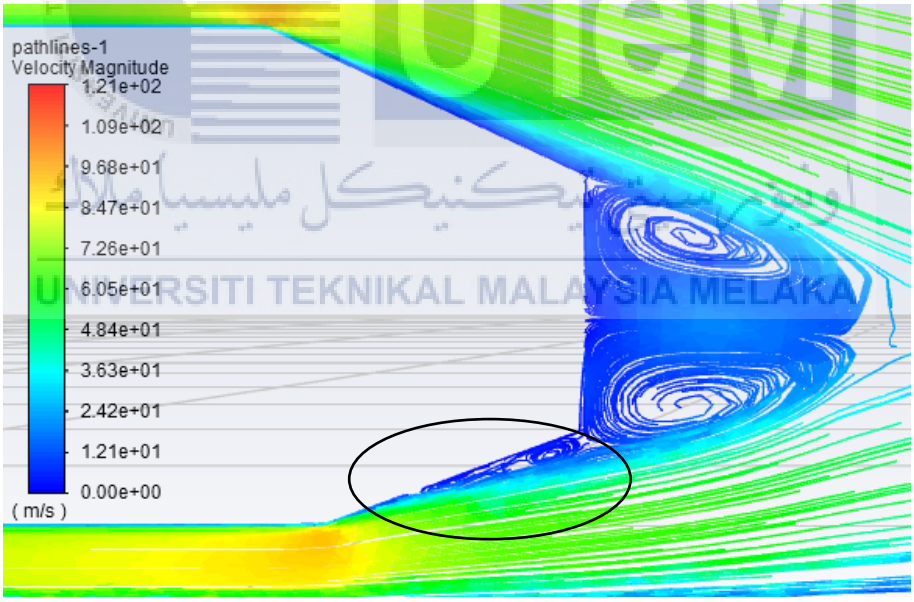

Figure 4.13: Flow separation zone generated at the diffuser of Ahmed body.

4.3 Simulation Results of Simplified 2D Model Analysis

Simplified 2D model analysis is done to evaluate the drag and lift coefficient on the 2D state of the model by using a simplified 2D midplane of the car body. The results of the drag and lift coefficient on different diffuser angle is tabulated in Table 4.7. Drag force occurs due to the stagnation of air pressure at the front part of the car body as shown in Figure 4.16. The front part of the car body has the highest pressure thus slows down the car body from moving forward. Based on the results shown in Figure 4.14, the lowest drag coefficient achieved at diffuser angle of 14 ° with drag coefficient of 2.1153. Starting diffuser angle of 16 °, the drag coefficient started to rise. This happens due to the formation of vortices at the diffuser which increases the drag force. By comparing Figure 4.18 with Figure 4.19, the vortices formed on diffuser with angle of 16 ° is more compact compared to vortices formed on diffuser with angle of 14 °, thus producing more drag force.

For the CFD simulation results of life coefficient obtained, the lowest lift coefficient achieved at the diffuser angle of 8 °. According to Figure 4.15, the lift coefficient decreases drastically from diffuser angle of 0 ° to 8 °, then increases slowly from 8 ° to 20 °. However according to most of the previous research, the lift coefficient should have a decreasing trend with increasing diffuser angle due to the increasing air flow velocity at bottom of the model. The inaccuracy of results obtained for lift coefficient may be due to the insufficient information provided in the 2D analysis as air flow from both side of model is not considered in the simulation. Besides, 2D analysis not able to represent the actual condition of the real simulation.

Table 4.7: CFD simulation result of simplified 2D model analysis.

diffuser angle (°)	drag coefficient	lift coefficient
0	2.1232	3.5800
2	2.1178	1.8272
4	2.1208	0.9017
6	2.1244	0.4286
8	2.1249	0.2746
10	2.1282	0.3342
12	2.1277	0.4972
14	2.1153	0.6105
16	2.1227	0.8659
18	2.1172	1.1008
20	2.1169	1.3344

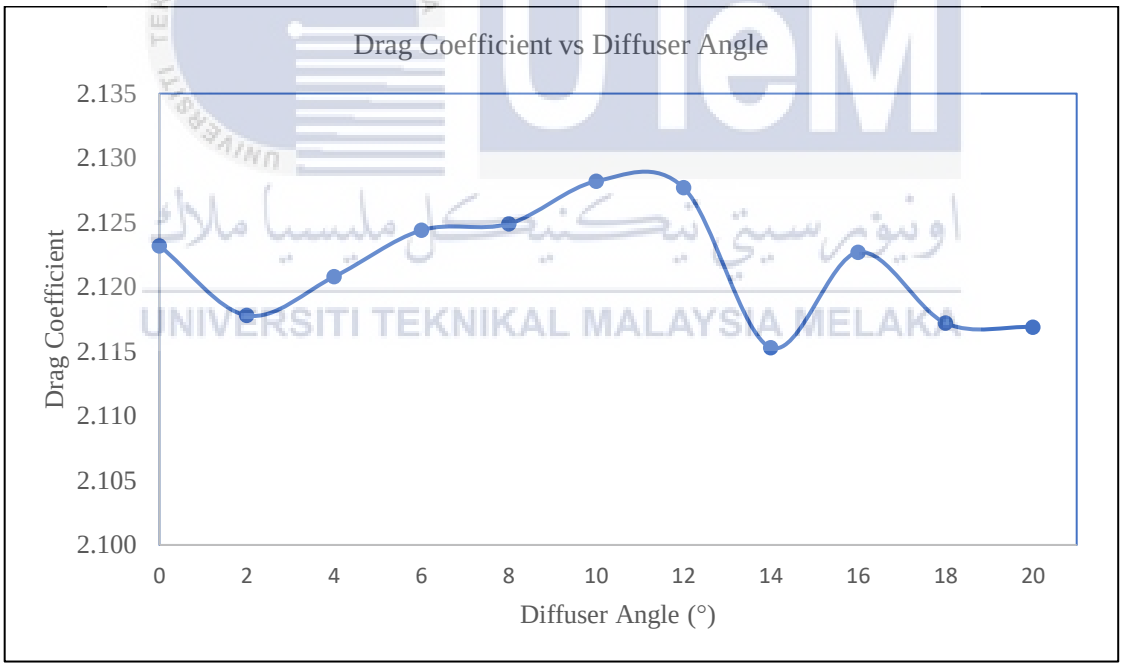

Figure 4.14: Graph of drag coefficient vs diffuser angle of simplified 2D model analysis.

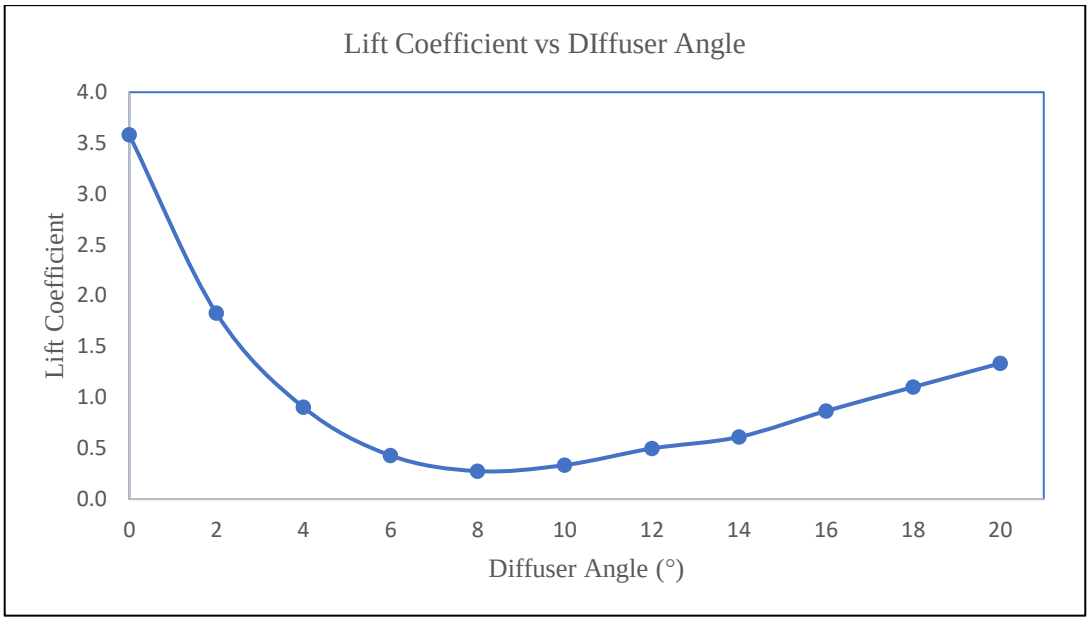

Figure 4.15: Graph of lift coefficient vs diffuser angle of simplified 2D model analysis.

Figure 4.16: Static pressure of simplified 2D model analysis.

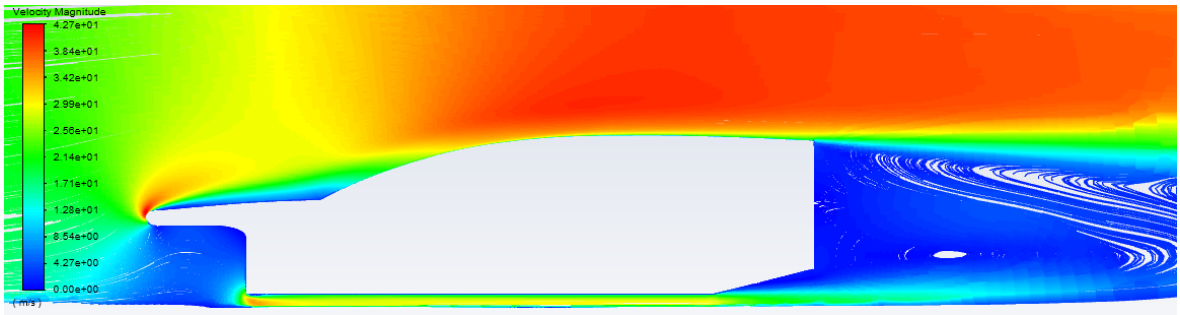

Figure 4.17: Velocity pathline of simplified 2D model analysis at diffuser angle of 14 °.

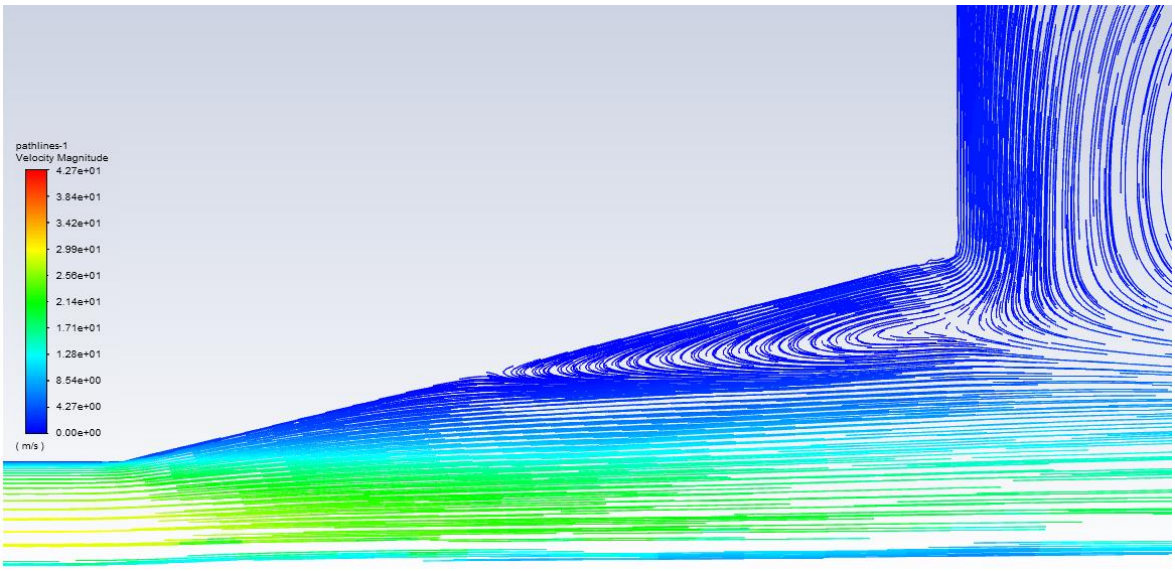

Figure 4.18: Velocity pathline formed at diffuser with angle of 14 °.

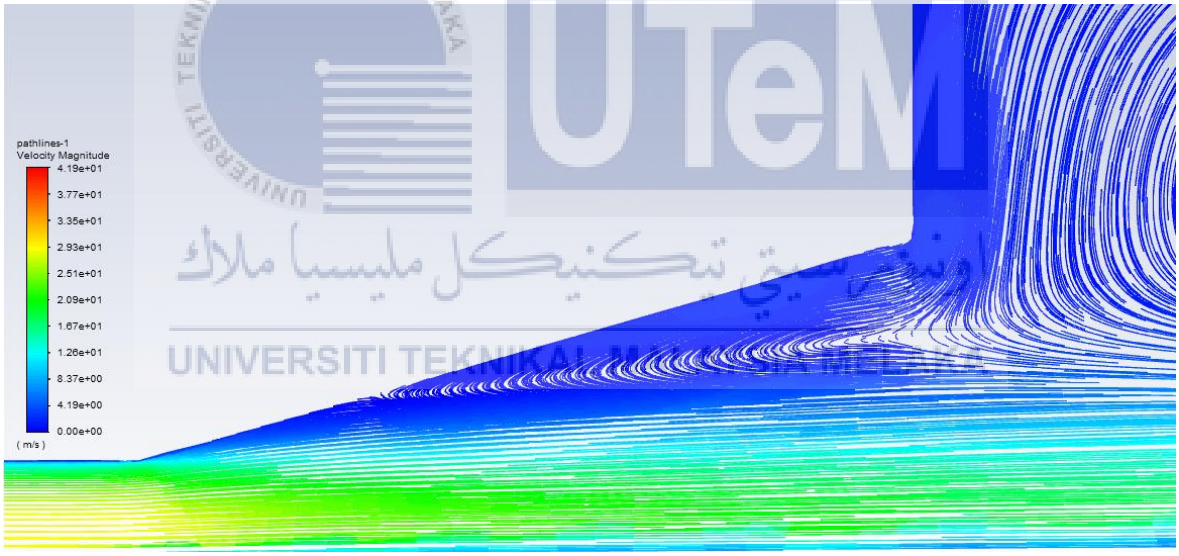

Figure 4.19: Velocity pathline formed at diffuser with angle of 16 °.

4.4 Simulation Results of Simplified 3D Model Analysis

Simplified 3D model analysis is done with the absence of a few components on the car model. The components are front and rear wings, wheel and axle. This is to exclude the aerodynamic effect caused by the wings. The CFD simulation results obtained is tabulated at Table 4.8. According to Figure 4.20, the drag coefficient decreases from diffuser angle of 0 ° and achieved lowest drag coefficient at diffuser angle of 10 ° with the drag coefficient of 0.6954. Then, the drag coefficient increases from 10 ° to 20 ° which shows the same trend as simulation results conducted on Ahmed body analysis. The increase of drag coefficient is explained by formation of vortices under the diffuser creating additional drag force on the rear part of model. By comparing Figure 4.22 and Figure 4.23, the vortices formed on the rear part of the model with diffuser angle 0 ° is greater than vortices formed on the model with diffuser angle of 10 °. Besides, the vortices formed on model with diffuser angle of 10 ° is affected by the inclined diffuser. Air flow from the bottom of model is redirected into the rear part of model by the diffuser thus causing the vortices formed to be smaller.

For the CFD simulation results for lift coefficient, the results obtained has a decreasing trend from diffuser angle of 0 ° to 20 ° which has the same decreasing trend as simulation results conducted on Ahmed body analysis. According to Figure 4.21, the lowest lift coefficient achieved at diffuser angle of 20 ° with the lift coefficient of 0.5062. By comparing Figure 4.24 and Figure 4.25, the air flow velocity at the bottom of model with diffuser angle of 20 ° is greater than model with diffuser angle of 0 °. The air flow velocity at the bottom of model with diffuser angle of 0 ° is around 16.43 m/s while model with diffuser angle of 20 ° has air flow velocity around 22.57 m/s. Since the air flow velocity at diffuser angle of 20 ° is higher, the pressure at the bottom of model is lower. Thus, the model will experience decrease of lift coefficient with the decrease of pressure under the model according to the Bernoulli's Principles.

Table 4.8: CFD simulation results of simplified 3D model analysis.

diffuser angle (°)	drag coefficient	lift coefficient
0	0.7307	0.7361
2	0.7238	0.6670
4	0.7135	0.6461
6	0.7073	0.6071
8	0.6999	0.5763
10	0.6954	0.5575
12	0.6965	0.5381
14	0.7005	0.5333
16	0.7047	0.5222
18	0.7065	0.5151
20	0.7124	0.5062

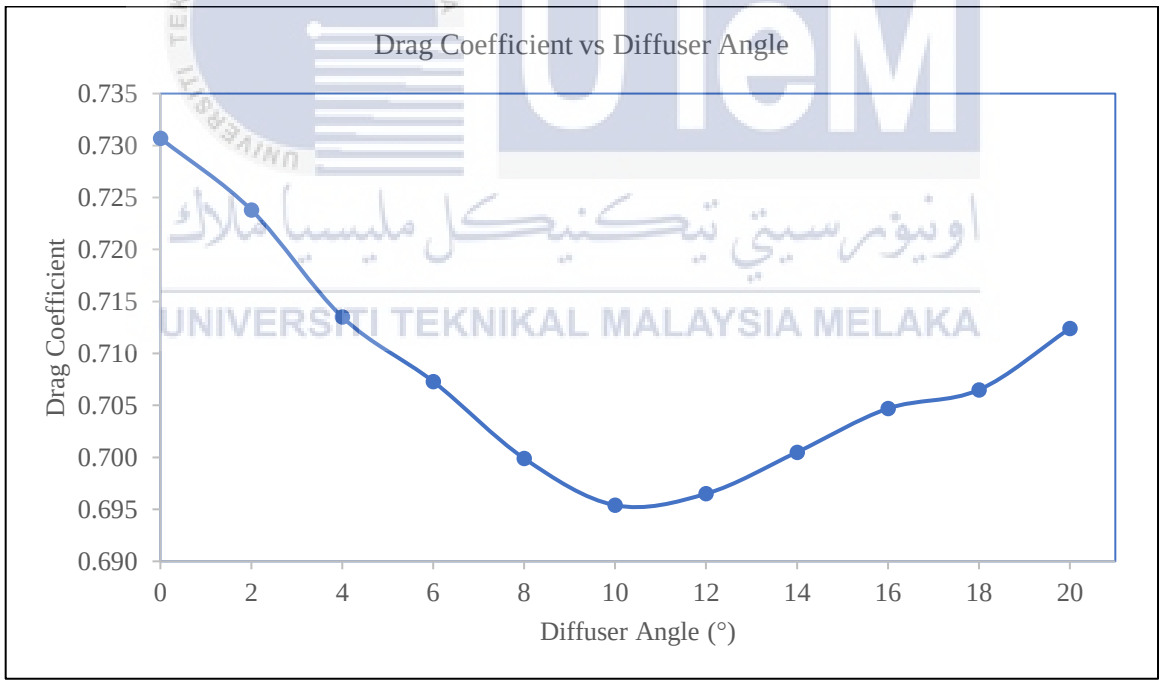

Figure 4.20: Graph of drag coefficient vs diffuser angle of simplified 3D model analysis.

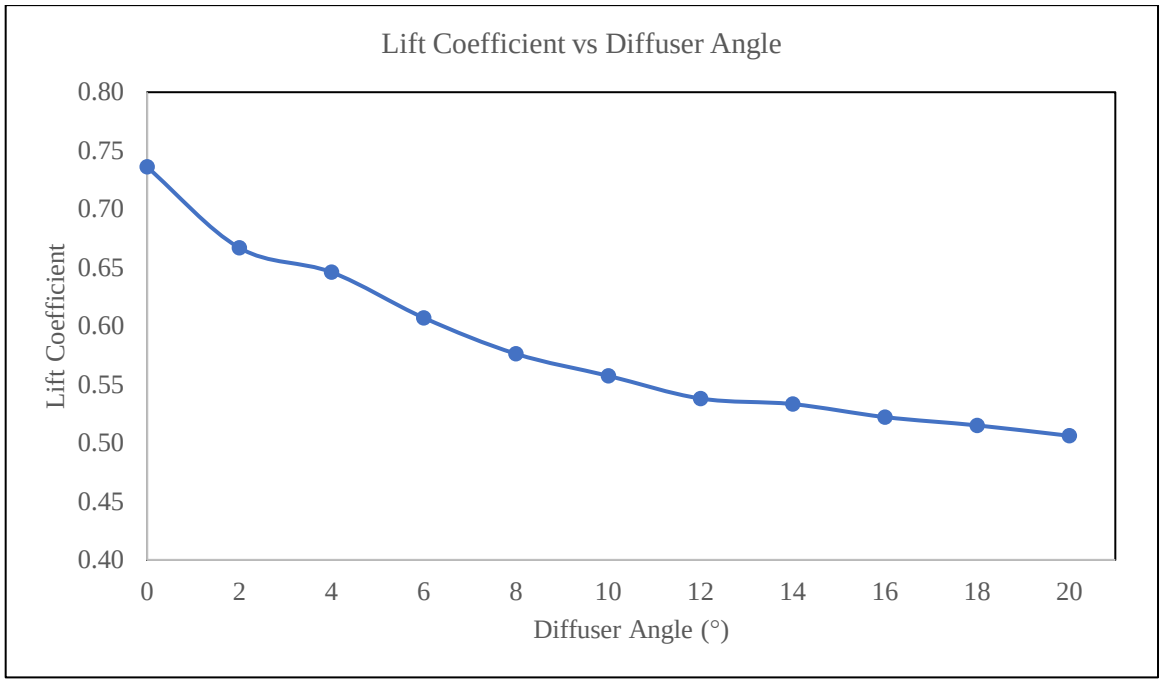

Figure 4.21: Graph of lift coefficient vs diffuser angle of simplified 3D model analysis.

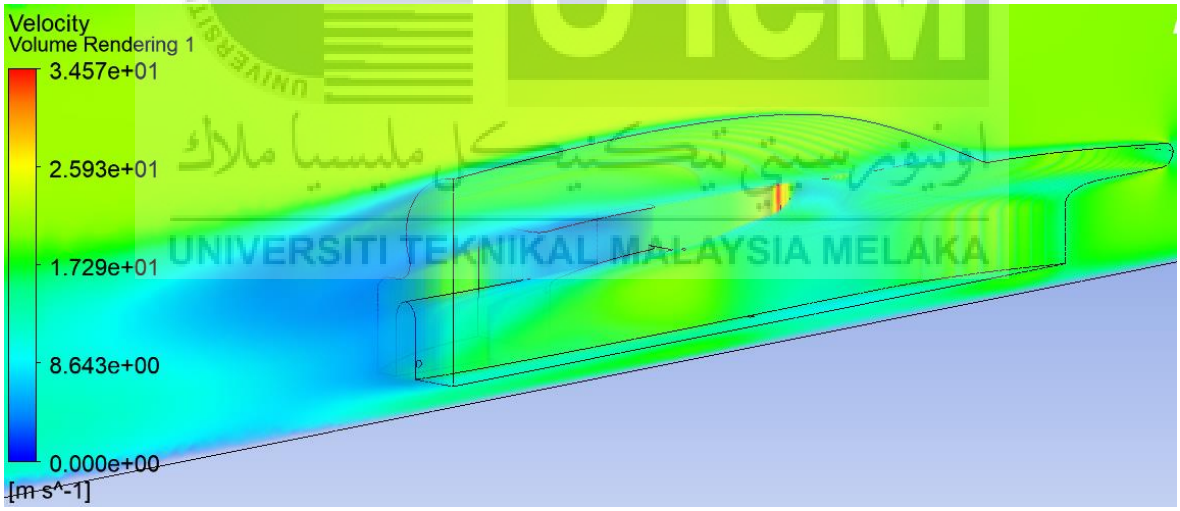

Figure 4.22: Air flow velocity of the simplified 3D model at diffuser angle of 0 °.

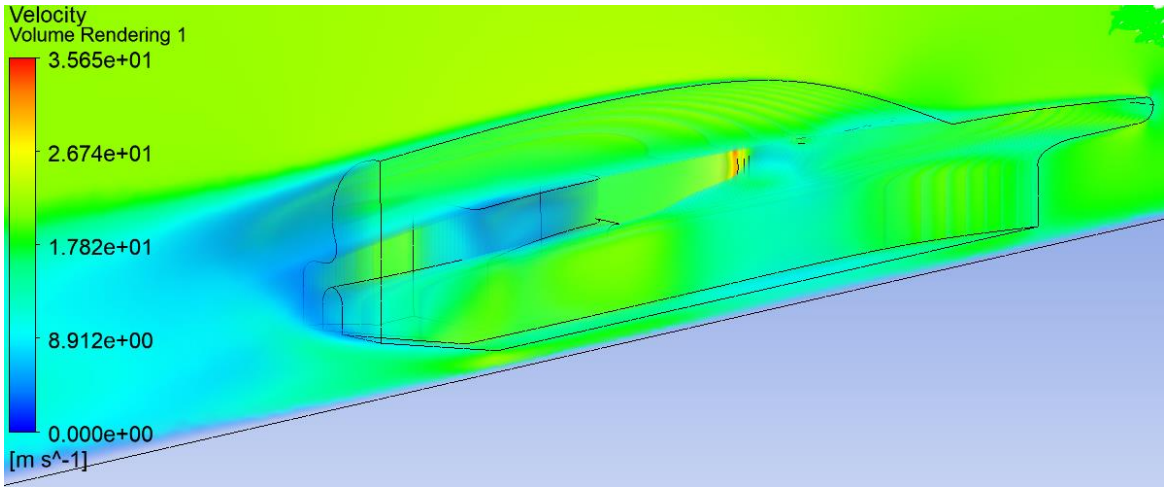

Figure 4.23: Air flow velocity of the simplified 3D model at diffuser angle of 10 °.

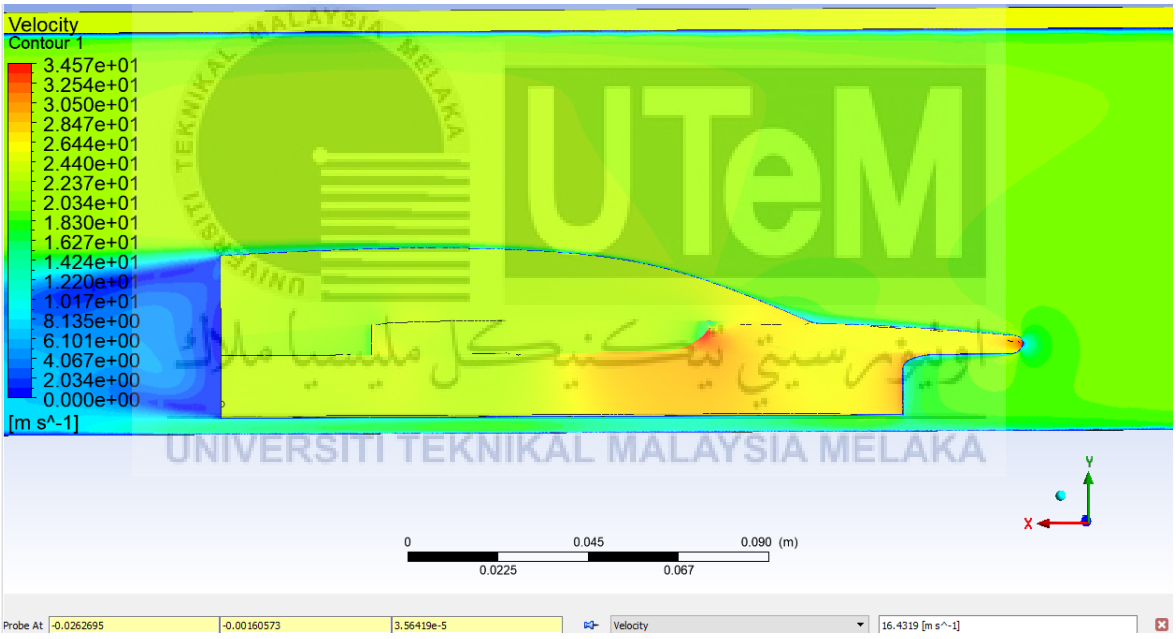

Figure 4.24: Air flow velocity at the bottom of simplified 3D model at diffuser angle of 0 °.

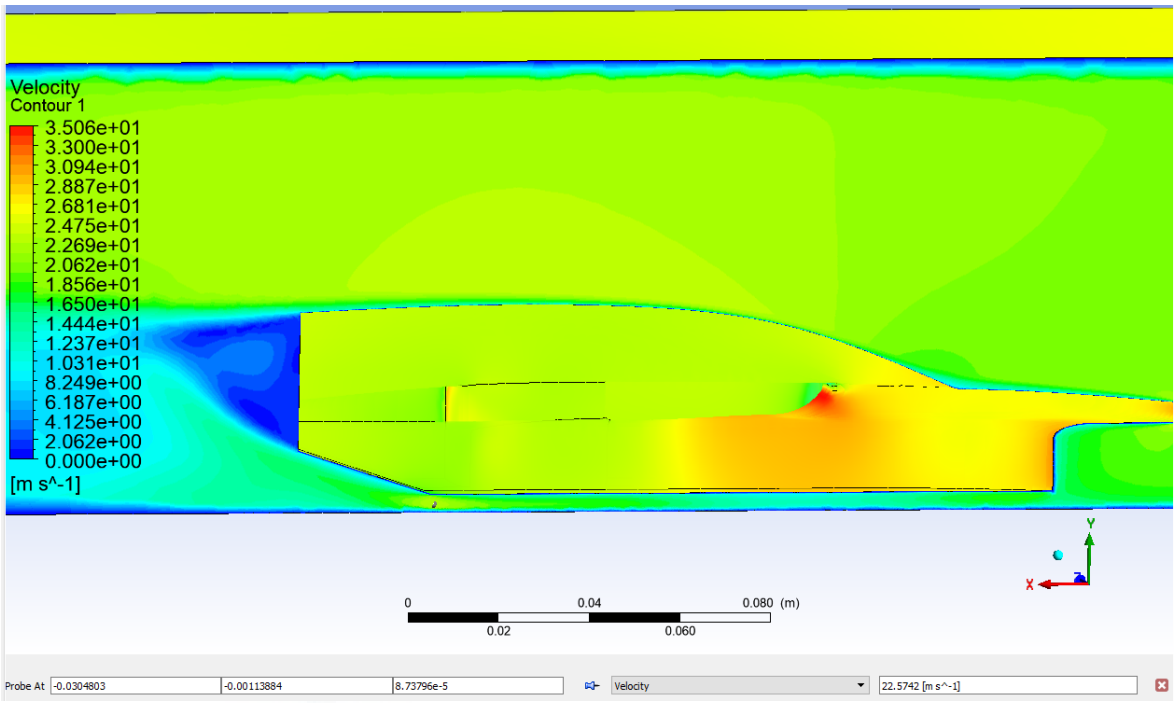

Figure 4.25: Air flow velocity at the bottom of simplified 3D model at diffuser angle of 20 °.

4.5 Simulation Results of Complete 3D Model Analysis

Complete 3D model analysis is done with full set of components installed on the model which includes front and rear wings, wheel and axle. The CFD simulation results for complete 3D model analysis is tabulated in Table 4.9. According to Figure 4.26, the lowest drag coefficient achieved on diffuser angle of 8 ° with the value of 1.6462. Then, the drag coefficient rises form 10 ° to 20 °. By comparing Figure 4.28 with Figure 4.29, vortices formed on the rear part of model at diffuser angle of 0 ° is greater than on the rear part of model at diffuser angle of 8 °. This causes model with diffuser angle of 8 ° has lower drag coefficient. However, starting at diffuser angle of 10 °, the outer part of diffuser which near to the wheel section started to form vortices which provides additional drag force. Figure 4.30 shows the vortices formed under the diffuser near to the wheel section at diffuser angle of 8 ° has lesser vortices formed compared to Figure 4.31 which shows more vortices formed at diffuser angle of 20 °. This condition increases the drag force on the rear part of model which slows down the model.

For the CFD simulation results of lift coefficient, the results obtained has the same decreasing trend with the increasing of diffuser angle. However, the overall lift coefficient has increased comparing to the lift coefficient of simplified 3D model analysis. This is due to additional aerodynamic components into the model. Both front and rear wings added has increased the lift coefficient. According to Figure 4.27, diffuser with angle of 20 ° has the lowest lift coefficient with the value of 3.0429. By comparing Figure 4.32 with Figure 4.33, air flow velocity at the bottom of model with diffuser angle of 20 ° is greater than model with diffuser angle of 0 °. Model with diffuser angle of 0 ° has air flow velocity around 18.54 m/s at the diffuser part while model with diffuser angle of 20 ° has air flow velocity around 22.65 m/s at the diffuser part. The air flow velocity increases with the increase of diffuser angle. Thus, causing the pressure under the model decreases according to the Bernoulli's Principles which decreases the lift coefficient.

Table 4.9: CFD simulation results of complete 3D model analysis.

diffuser angle (°)	drag coefficient	lift coefficient
0	1.6563	3.1703
2	1.6528	3.1434
4	1.6483	3.1170
6	1.6468	3.1019
8	1.6462	3.0854
10	1.6485	3.0753
12	1.6504	3.0581
14	1.6541	3.0568
16	1.6560	3.0447
18	1.6610	3.0445
20	1.6685	3.0429

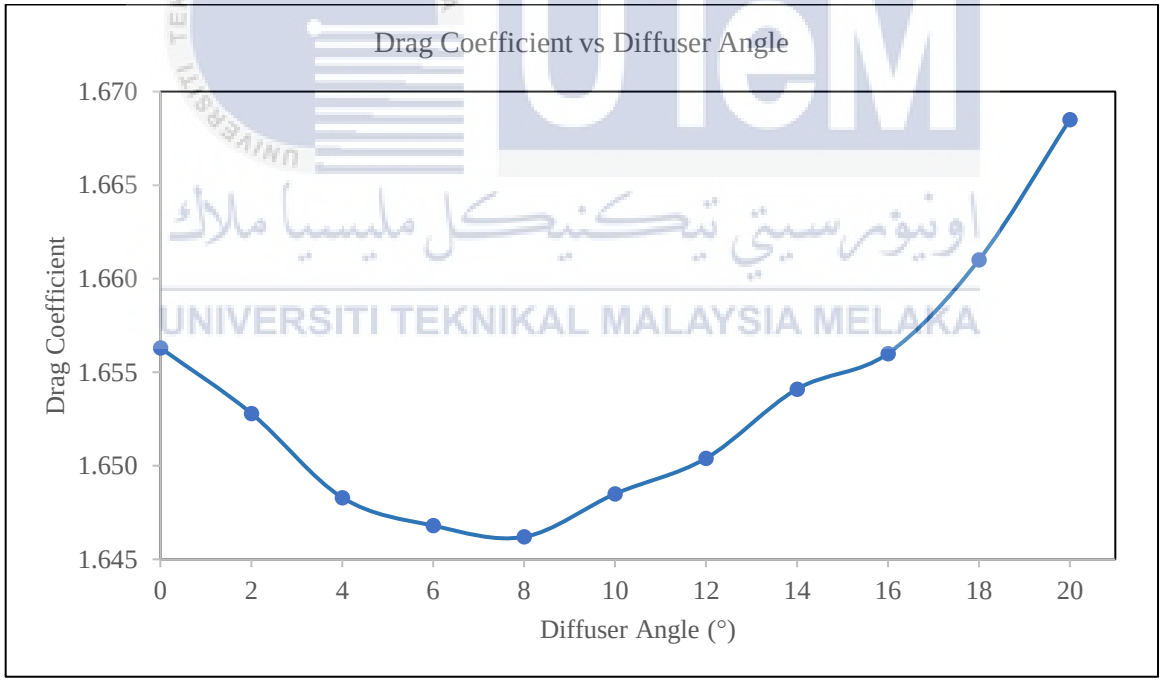

Figure 4.26: Graph of drag coefficient vs diffuser angle of complete 3D model analysis.

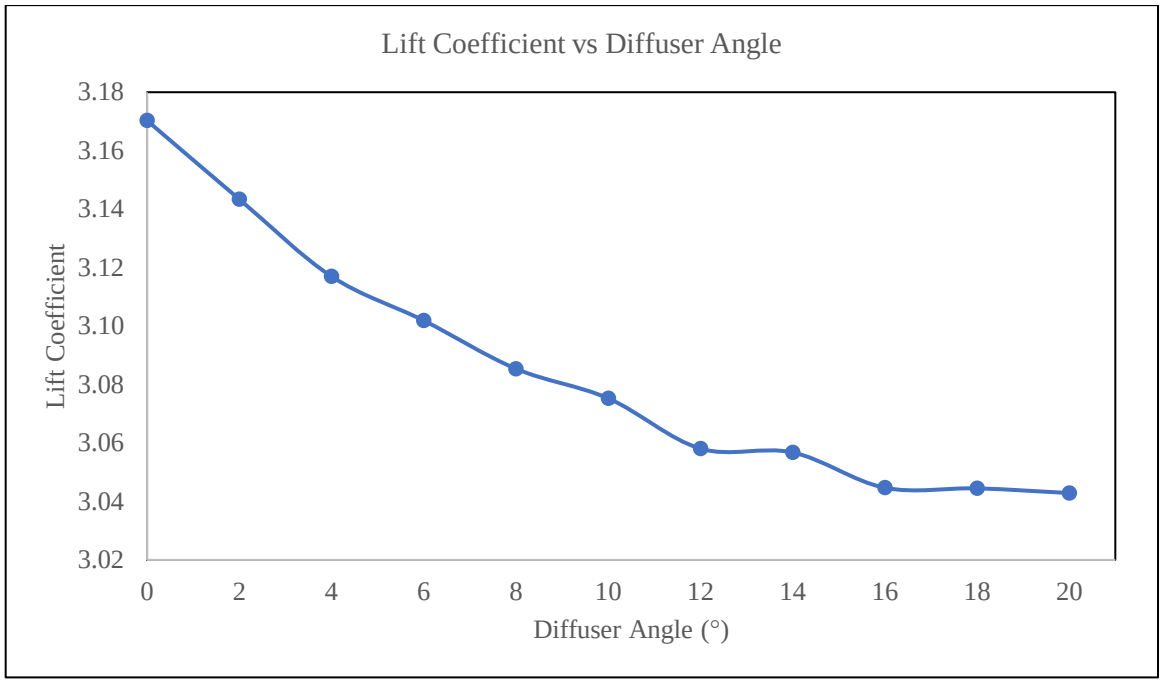

Figure 4.27: Graph of lift coefficient vs diffuser angle of complete 3D model analysis.

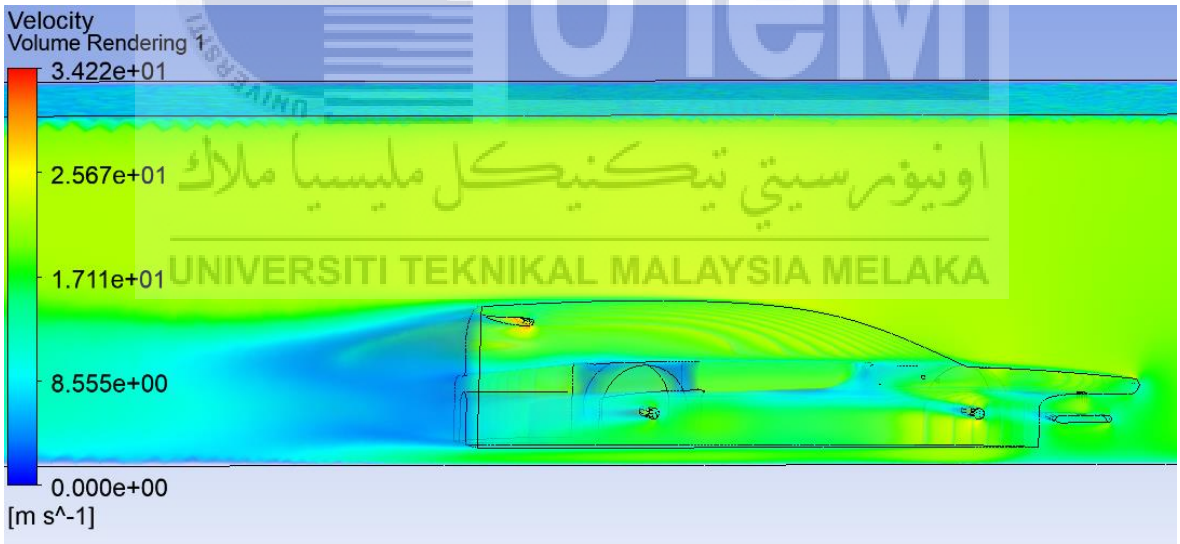

Figure 4.28: Air flow velocity of the complete 3D model at diffuser angle of 0 °.

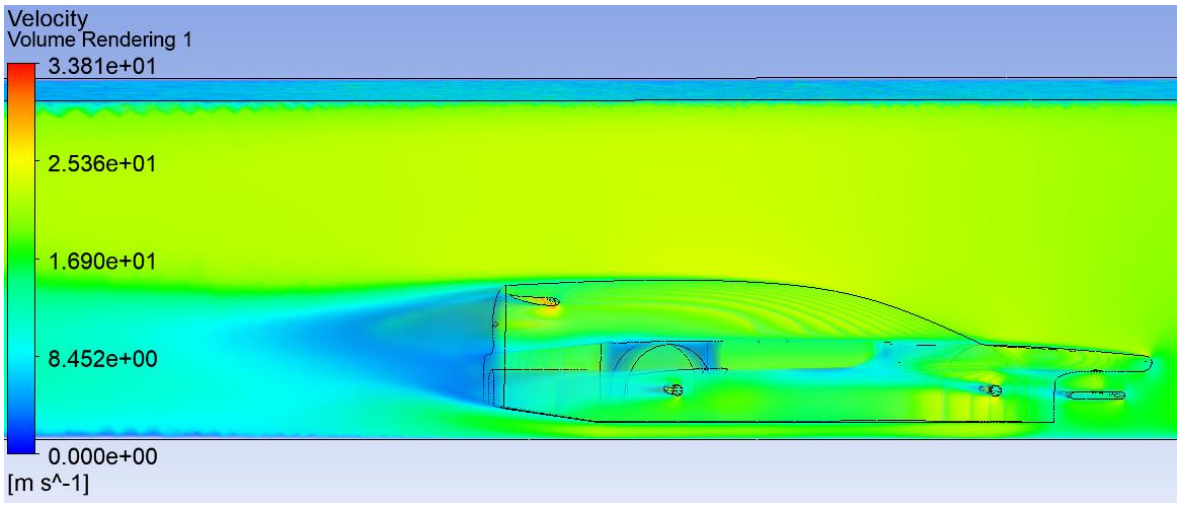

Figure 4.29: Air flow velocity of the complete 3D model at diffuser angle of 8 °.

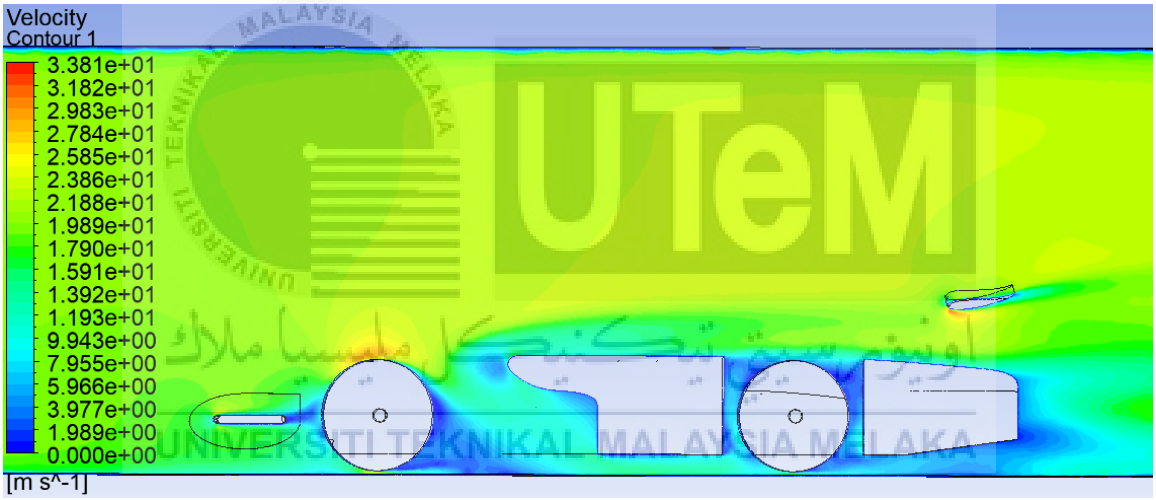

Figure 4.30: Air flow velocity at the wheel section of the complete 3D model at diffuser angle of 8 °.

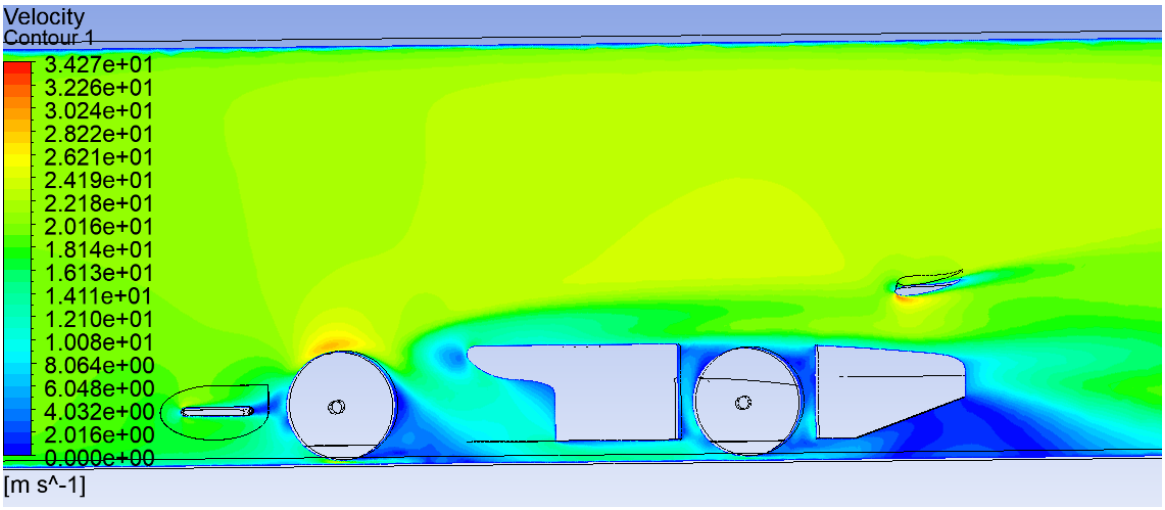

Figure 4.31: Air flow velocity at the wheel section of the complete 3D model at diffuser angle of 20 °.

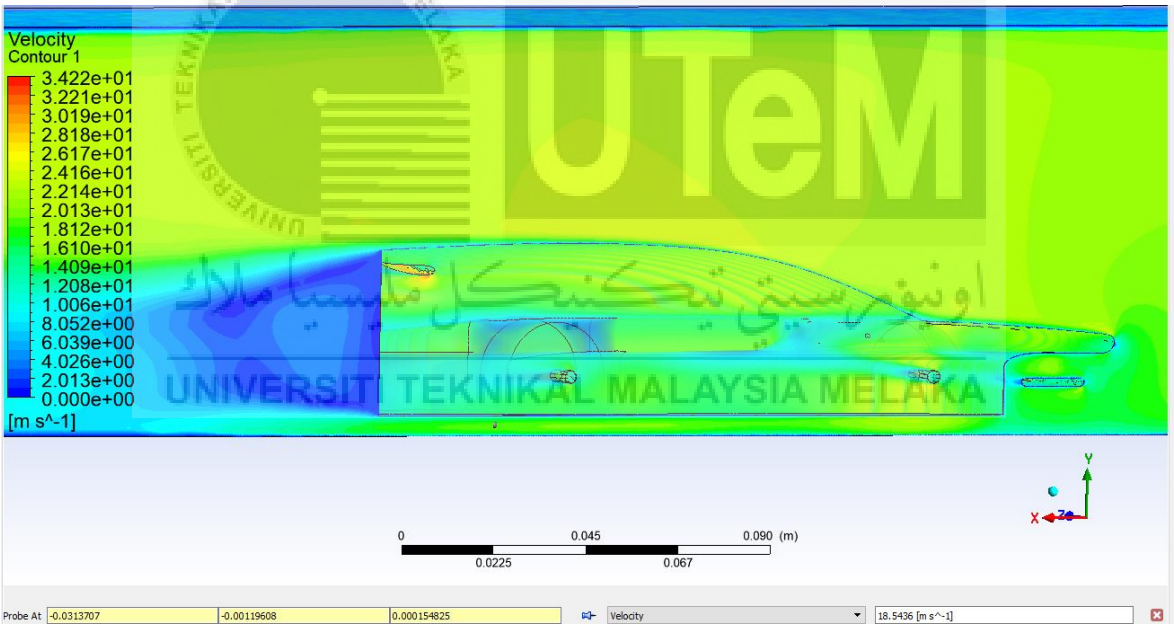

Figure 4.32: Air flow velocity at the bottom of the complete 3D model at diffuser angle of 0 °.

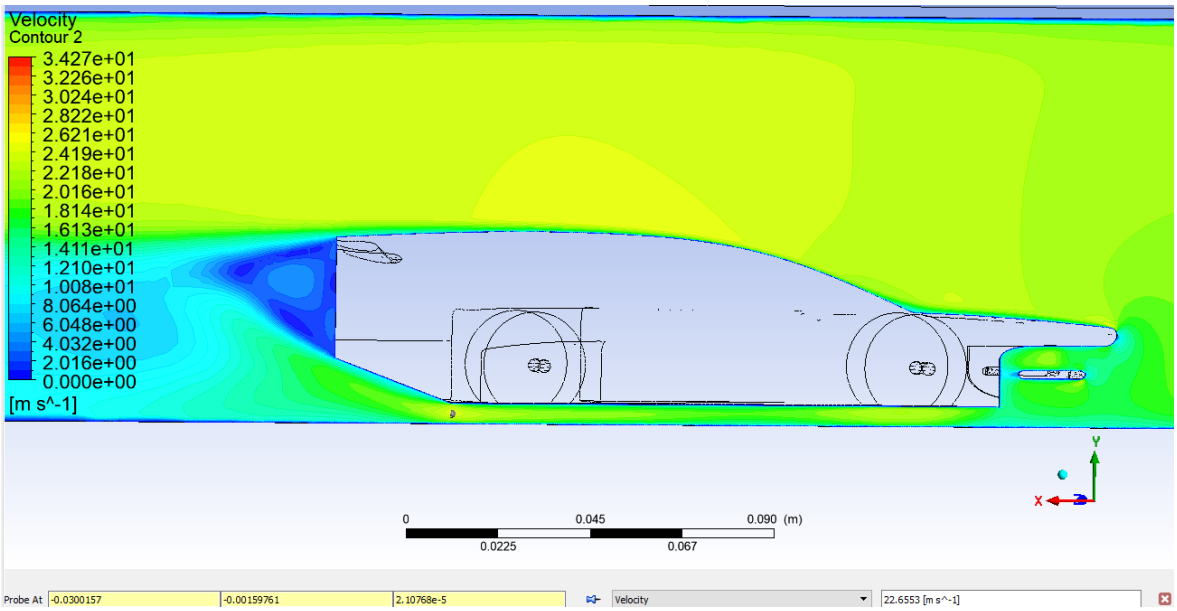

Figure 4.33: Air flow velocity at the bottom of the complete 3D model at diffuser angle of 20 °.

4.5.1 CFD simulation results of complete 3D model analysis without sidepot

The analysis is done to compare the CFD simulation results of complete 3D model with complete 3D model without sidepot. Table 4.10 shows the CFD simulation results of complete 3D model analysis with sidepot and without sidepot. Based on the table, the effect on the drag coefficient with the model without sidepot is relatively small compared to the model with sidepot. The overall drag coefficient of model without sidepot is 0.2551 % to 1.6073 % smaller than the model with sidepot. According to Figure 4.34, the drag coefficient of model without sidepot shows increasing trend from 0 ° to 16 °. This is because air flow through the front wheel is blocked due to the absence of sidepot which cause extra stagnation of pressure on the front part of model. Model with sidepot able to redirect the air flow through the path of sidepot into the rear part of model which will eliminates the occurs of pressure stagnation.

According to Figure 4.35, the overall lift coefficient of model without sidepot is relatively small compared to model with sidepot. However, the percentage difference is

between both model for lift coefficient is in-between 13.9867 % to 16.7783 % which means the presence of sidepot has great influence on the lift coefficient. By comparing Figure 4.36 with Figure 4.37, the air flow velocity at the bottom of model without sidepot has higher air flow velocity than the model with sidepot. With the existence of sidepot, this allows more space for air flow at the bottom the model thus lowering the air flow velocity. This cause the pressure at the bottom of the model without sidepot to be lower and has lower lift coefficient.

Table 4.10: CFD simulation results of complete 3D model analysis without sidepot.

diffuser angle (°)	C_D with sidepot	C_D without sidepot	C_D percentage difference (%)	C_L with sidepot	C_L without sidepot	C_L percentage difference (%)
0	1.6563	1.6301	1.6073	3.1703	2.7148	16.7783
2	1.6528	1.6311	1.3304	3.1434	2.6667	17.8760
4	1.6483	1.6307	1.0793	3.1170	2.6553	17.3878
6	1.6468	1.6377	0.5556	3.1019	2.6550	16.8323
8	1.6462	1.6379	0.5067	3.0854	2.6473	16.5489
10	1.6485	1.6437	0.2920	3.0753	2.6560	15.7868
12	1.6504	1.6462	0.2551	3.0581	2.6686	14.5956
14	1.6541	1.6491	0.3031	3.0568	2.6734	14.3412
16	1.6560	1.6519	0.2481	3.0447	2.6711	13.9867
18	1.6610	1.6494	0.7032	3.0445	2.6689	14.0732
20	1.6685	1.6498	1.1334	3.0429	2.6663	14.1244

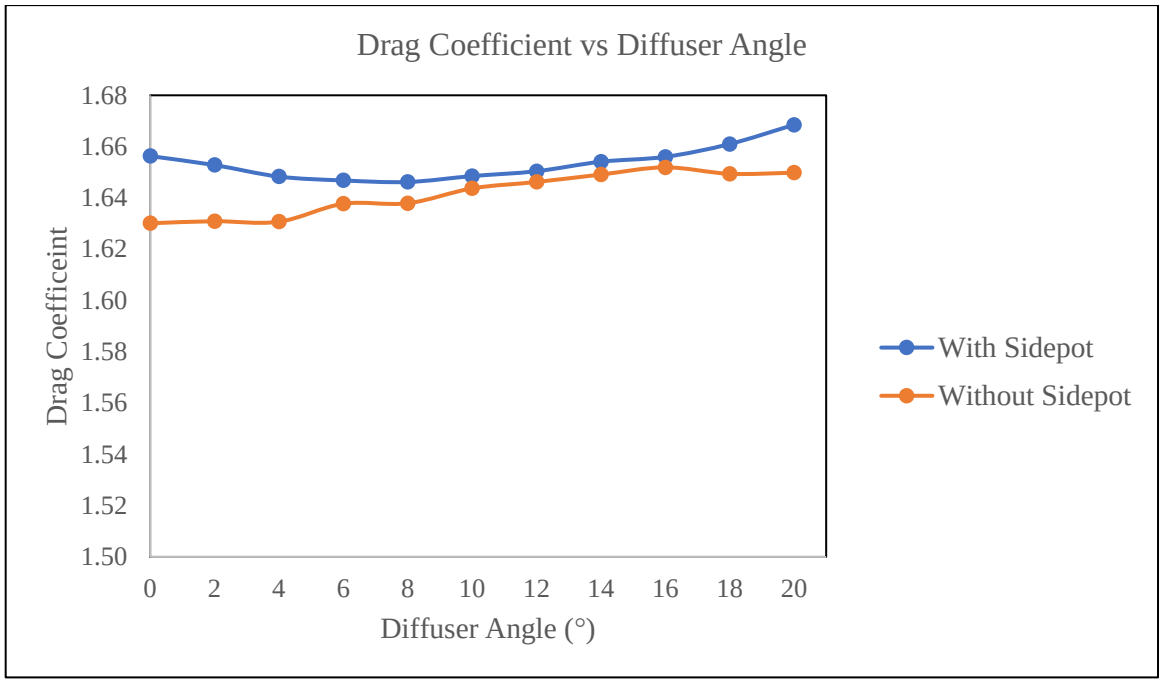

Figure 4.34: Graph of drag coefficient vs diffuser angle for model with sidepot and without sidepot.

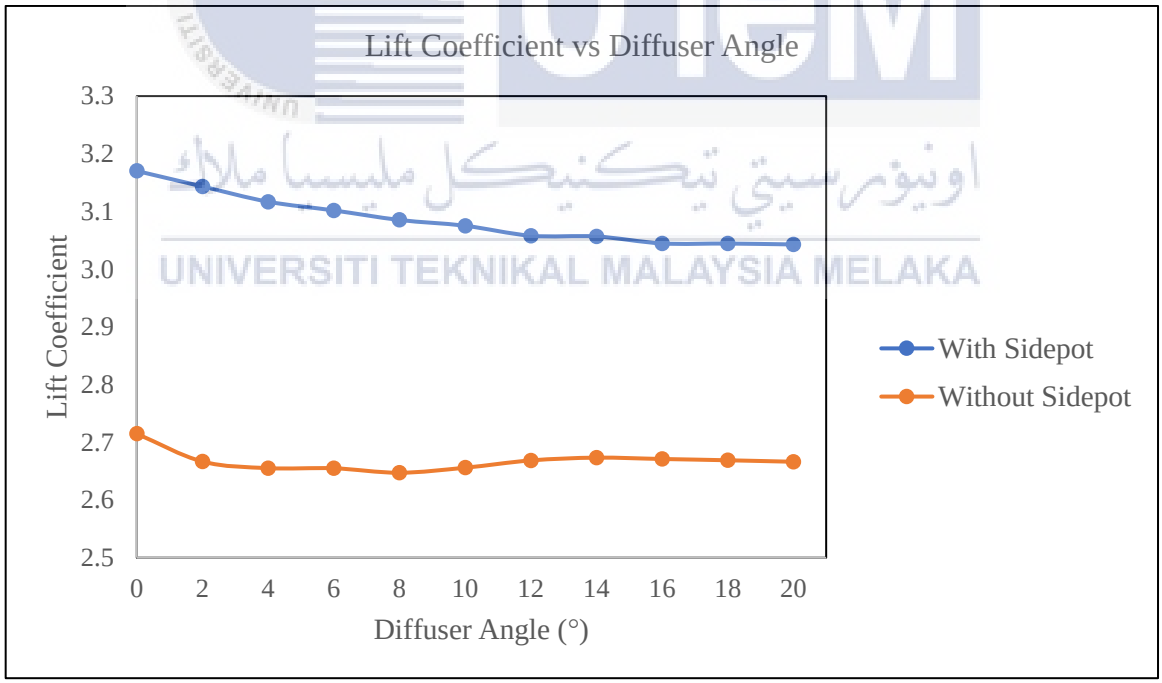

Figure 4.35: Graph of lift coefficient vs diffuser angle for model with sidepot and without sidepot.

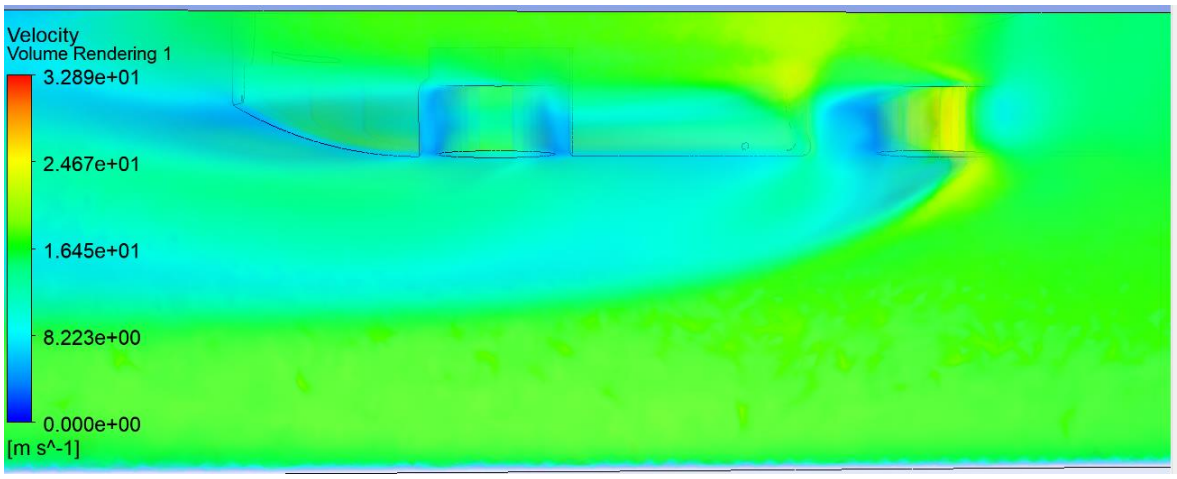

Figure 4.36: Air flow velocity at the bottom of complete 3D model without sidepot at diffuser angle of 0 °.

Figure 4.37: Air flow velocity at the bottom of complete 3D model with sidepot at diffuser angle of 0 °.

CHAPTER 5
CONCLUSION AND RECOMMENDATION

In this report, 3D model of F1 IN SCHOOLS Car model is designed with different angle of diffuser to test its aerodynamic behaviour at high speed. Before running the CFD simulation of the model, a few tests were conducted to ensure the accuracy of results generated. The first is mesh density analysis which is conducted to make sure results generated is independent of the density of mesh. The next is verification of Fluent solver settings by comparing own CFD simulation results with previous wind tunnel test result to verify the suitability of selected Fluent solver settings. Then, own CFD simulation results for Ahmed body were compared with simulation results done previously to check its percentage difference for validation of Fluent solver settings' accuracy. After that, CFD simulation of Ahmed body is repeated with different values of diffuser angle to compare its aerodynamic effect with Ahmed body without diffuser. After test is done, CFD simulation is started with simplified 2D model analysis, followed by simplified 3D model analysis, then complete 3D model analysis and lastly complete 3D model analysis without sidepot. Throughout the analysis, drag and lift coefficient is studied with the air flow behaviour around the model.

For simplified 2D model analysis, the ideal solution selected is diffuser angle of 14 ° which has lowest drag coefficient of 2.1153 and lift coefficient of 0.6105. However, the results obtained is less reliable due to insufficient information provided on the model for CFD simulation. For simplified 3D model analysis, the ideal solution selected is diffuser angle of 10 ° which has lowest drag coefficient of 0.6954 and lift coefficient of 0.5575. For the complete 3D model analysis, the ideal solution selected is diffuser angle of 8 ° with the

drag coefficient of 1.6462 and lift coefficient of 3.0753. By comparing simplified 3D model analysis with complete 3D model analysis, the overall drag coefficient has increased in the CFD results obtained for complete 3D model analysis. This is because more aerodynamic components added to the model which provides additional drag force such as front and rear wings, wheels and axles. Vortices formed behind those components during high speed and slows down the model. For the simulation result of complete 3D model without sidepot, both model is compared to study the air flow behaviour at the bottom of model. Model with sidepot able to redirect the vortices formed behind the front wheel into the rear part of model which also refilling the vacuum area on the rear part of model. Besides, it also reduces the stagnation of air pressure at the front part of model. The air flow velocity of model with diffuser has lower velocity compared to model without sidepot. This causes the model with sidepot to have lower lift coefficient than model without sidepot.

Since manipulating the diffuser angle will only shows decreasing trend for lift coefficient, the recommendation to achieve the suitable aerodynamic conditions for the fast-moving F1 IN SCHOOLS Car is to have the least drag coefficient and suitable lift coefficient. According to the literature review and results generated, diffuser angle starting from range 8 ° to 14 ° are estimated to give optimum result for drag coefficient. The results obtained from the CFD simulation of complete 3D model analysis have the lift coefficient within the range of 3.0429 to 3.1703 while drag coefficient is within the range of 1.6462 to 1.6685. It is noticeable that the manipulating the diffuser angle on the has only small effect on both drag and lift coefficient. Thus, to achieve a better aerodynamic performance on the model moving in high speed, the study of the design of front and rear wings and the car body are significant. This is because front and rear wings play an important role controlling the lift coefficient of the model while the aerofoil shape of the car body can also be further improved to reduce the stagnation of air pressure on the car body. Besides, recommendations on further study regarding the effect of sidepot on car body is also required. This is because presence of sidepot has noticeable changes on the lift coefficient. Besides, additional of sidepot also decrease the turbulent formed on the rotating wheel. Thus, modification on sidepot in terms of external shape, internal flow tunnel shape, inlet and outlet position and more is important in determining the aerodynamic performance of the model.

For the accuracy of the CFD results generated, wheel's angular velocity can be included to generate a more accurate results since the rotation on the wheels might changes the behaviour of air flow around the model. Besides, the CFD simulation result can also be compared with wind tunnel test results for accuracy validations.

REFERENCES

Abid, M., Wajid, H. A., Iqbal, M. Z., Najam, S., Arshad, A., & Ahmad, A. (2017). Design and analysis of an aerodynamic downforce package for a Formula Student Race Car. *IIUM Engineering Journal*, *18*(2), 212–224. https://doi.org/10.31436/iiumej.v18i2.679

Abu Mansor, M. R., & Harun, Z. (2018). F1 in SCHOOLS Competition to Promote STEM: Aerodynamic Investigation of Miniature F1 in SCHOOLS Car. *Proceedings - 2017 7th World Engineering Education Forum, WEEF 2017- In Conjunction with: 7th Regional Conference on Engineering Education and Research in Higher Education 2017, RCEE and RHEd 2017, 1st International STEAM Education Conference, STEAMEC 201*, 708–712. https://doi.org/10.1109/WEEF.2017.8467172

Corke, T. C., & Thomas, F. O. (2018). Active and passive turbulent boundary-layer drag reduction. *AIAA Journal*, *56*(10), 3835–3847. https://doi.org/10.2514/1.J056949

Dong, T., Minelli, G., Wang, J., Liang, X., & Krajnović, S. (2020). The effect of ground clearance on the aerodynamics of a generic high-speed train. *Journal of Fluids and Structures*, *95*, 102990. https://doi.org/10.1016/j.jfluidstructs.2020.102990

Džijan, I., Pašić, A., Buljac, A., & Kozmar, H. (2019). Aerodynamic forces acting on a race car for various ground clearances and rake angles. *Journal of Applied Fluid Mechanics*, *12*(2), 361–368. https://doi.org/10.29252/jafm.12.02.28706

Eftekhari, H., Al-Obaidi, A. S. M., & Eftekhari, S. (2020). The effect of spoiler shape and setting angle on racing cars aerodynamic performance. In *Indonesian Journal of Science and Technology* (Vol. 5, Issue 1, pp. 11–20). https://doi.org/10.17509/ijost.v5i1.22701

Euler equations (fluid dynamics) - Wikipedia. (, November). https://en.wikipedia.org/wiki/Euler_equations_(fluid_dynamics)#History

F1 In Schools. (2020). *F1 in Schools™ - World Finals 2020 Technical Regulations*. https://www.f1inschools.com/uploads/1/1/8/9/118908723/f1s_wf_2020_technicall_regulations__updated_cover_.pdf

Feng, Q., Luo, B., Zhang, H., Peng, H., Zhu, Z., Ding, Z., Zhu, L., Xie, W., Li, B., & Zhao, X. (2020). Optimization of the Aerodynamic Lift and Drag of LYNK&CO 03+ with Simulation and Wind Tunnel Test. *SAE Technical Papers*, *2020-April*(April). https://doi.org/10.4271/2020-01-0672

Fu, Y. F., Yuan, C. Q., & Bai, X. Q. (2017). Marine drag reduction of shark skin inspired riblet surfaces. *Biosurface and Biotribology*, *3*(1), 11–24. https://doi.org/10.1016/j.bsbt.2017.02.001

G. Yunqing, L. Tao, M. Jiegang, S. Zhengzan, Z. P. (2017). Analysis of drag reduction methods and mechanisms of turbulent. *Appl. Bionics Biomech.*, *2017*, 1--8.

Hassan, S. M. R., Islam, T., Ali, M., & Islam, M. Q. (2014). Numerical Study on Aerodynamic Drag Reduction of Racing Cars. *Procedia Engineering*, *90*, 308–313. https://doi.org/10.1016/j.proeng.2014.11.854

Hu, X., Zhang, R., Ye, J., Yan, X., & Zhao, Z. (2011). Influence of different diffuser angle on Sedan's aerodynamic characteristics. *Physics Procedia*, *22*, 239–245. https://doi.org/10.1016/j.phpro.2011.11.038

Huluka, A. W., & Kim, C. H. (2020). Effect of the air duct system of a simplified vehicle model on aerodynamic performance. *International Journal of Automotive and Mechanical Engineering*, *17*(2), 7985–7995. https://doi.org/10.15282/ijame.17.2.2020.17.0598

Huminic, A., & Huminic, G. (2020). Aerodynamics of curved underbody diffusers using CFD. *Journal of Wind Engineering and Industrial Aerodynamics*, *205*(August), 104300. https://doi.org/10.1016/j.jweia.2020.104300

Hwang, B. G., Lee, S., Lee, E. J., Kim, J. J., Kim, M., You, D., & Lee, S. J. (2016). Reduction of drag in heavy vehicles with two different types of advanced side skirts. *Journal of Wind Engineering and Industrial Aerodynamics*, *155*, 36–46. https://doi.org/10.1016/j.jweia.2016.04.009

ILLINOIS. (2020). *Applied Aerodynamics*. https://aerospace.illinois.edu/research/research-areas/applied-aerodynamics

Jameson, A. (2012). *Computational Fluid Dynamics Past, Present and Future*. http://aero-comlab.stanford.edu/Papers/NASA_Presentation_20121030.pdf

Kell, R. T. (2009a). *Aerodynamic Analysis of F1 in Schools Challenge Car Models*. 1–10.

Kell, R. T. (2009b). *Aerodynamic Analysis of F1 in Schools Challenge Car Models*. *1*(1), 1–10.

Khalil, E. E. (2012). CFD history and applications. *CFD Letters*, *4*(2), 43–46.

Kim, J. J., Lee, S., Kim, M., You, D., & Lee, S. J. (2017). Salient drag reduction of a heavy vehicle using modified cab-roof fairings. *Journal of Wind Engineering and Industrial Aerodynamics*, *164*(March 2016), 138–151. https://doi.org/10.1016/j.jweia.2017.02.015

Lee, S. W., & Kim, H. L. (2019). Numerical study of active aerodynamic control via flow discharge on a high-camber rear spoiler of a road vehicle. *Applied Sciences (Switzerland)*, *9*(22). https://doi.org/10.3390/app9224783

Meile, W., Brenn, G., Reppenhagen, A., Lechner, B., & Fuchs, A. (2011). Experiments and numerical simulations on the aerodynamics of the ahmed body. *CFD Letters*, *3*(1), 32–38.

Mierzejewska, P., Cieslinski, A., & Jodko, D. (2018). Influence of the diffuser on the drag coefficient of a solar car. *Mechanics and Mechanical Engineering*, *22*(2), 509–519. https://doi.org/10.2478/mme-2018-0041

Moghimi, P., & Rafee, R. (2018). Numerical and experimental investigations on aerodynamic behavior of the Ahmed body model with different diffuser angles. *Journal of Applied Fluid Mechanics*, *11*(4), 1101–1113. https://doi.org/10.29252/jafm.11.04.27923

Mosiężny, J., Ziegler, B., Grzymisławski, P., & Ślefarski, R. (2020). Base drag reduction concept for commercial road vehicles. *Energy*, *205*. https://doi.org/10.1016/j.energy.2020.118075

Paturrahman, M. F., Mansor, M. R. A., Harun, Z., & Sabri, M. A. M. (2018). Study on the modification effect of side pot and diffuser to the aerodynamics of the F1 IN SCHOOLS car. *International Journal of Engineering and Technology(UAE)*, *7*(3), 123–128. https://doi.org/10.14419/ijet.v7i3.17.16635

Plis, S. M., Ramirez, R., Sonntag, H., Piastra, M. C., Nüßing, A., Vorwerk, J., Bornfleth, H., Oostenveld, R., Engwer, C., & Wolters, C. H. (2018). The Discontinuous Galerkin

Finite Element Method for Solving the MEG and the Combined MEG/EEG Forward Problem. *Frontiers in Neuroscience*, *12*, 30. https://doi.org/10.3389/fnins.2018.00030

Razak, M. F. A. (2009). *A study of aerodynamics for F1 in schools*. Universiti Teknikal Malaysia Melaka.

S. J. Lim, M. R. A. M. (2017). Aerodynamic Analysis of F1 IN SCHOOLSTM Car. *Journal of the Society of Automotive Engineers Malaysia*, *1*(1), 41–54.

Singh, A., Jain, A., & Sharma, A. (2020). Designing a 3-D Model of Bodywork of a Vehicle with Low Coefficient of Drag and High Downforce. *Materials Today: Proceedings*, *28*, 2197–2204. https://doi.org/10.1016/j.matpr.2020.04.253

Sreeradh, V. M. (2018). Computational analysis of a sedan using computational fluid dynamics software. *International Journal of Mechanical and Production Engineering Research and Development*, *8*(3), 985–990. https://doi.org/10.24247/ijmperdjun2018104

Sucipto, S. A., & Widodo, W. A. (2018). *Numerical study of multiple-channel diffusers on the rear bus body Numerical Study of Multiple-Channel Diffusers on The Rear Bus Body*. *030094*(January 2017). https://doi.org/10.1063/1.4968347

Takahashi, H., Iijima, H., Kurita, M., & Koga, S. (2019). Evaluation of skin friction drag reduction in the turbulent boundary layer using riblets. *Applied Sciences (Switzerland)*, *9*(23). https://doi.org/10.3390/app9235199

Wang, J., Li, H., Liu, Y., Liu, T., & Gao, H. (2018). Aerodynamic research of a racing car based on wind tunnel test and computational fluid dynamics. *MATEC Web of Conferences*, *153*, 1–5. https://doi.org/10.1051/matecconf/201815304011

William L.Hosch. (2020, May 28). *Navier-Stokes equation*. Encyclopaedia Britannica. https://www.britannica.com/science/Navier-Stokes-equation

Zhang, L., Shan, X., & Xie, T. (2020). Active Control for Wall Drag Reduction: Methods, Mechanisms and Performance. *IEEE Access*, *8*, 7039–7057. https://doi.org/10.1109/ACCESS.2020.2963843